

## Analytical Chemistry

Optical pH sensor covering the range from pH 0–14 compatible with mobile-device readout and based on a set of rationally designed indicator dyes

Raúl Gotor, Pichandi Ashokkumar, Mandy Hecht, Karin Keil, and Knut Rurack\*

Chemical and Optical Sensing Division, Bundesanstalt für Materialforschung und –prüfung (BAM),  
Richard-Willstätter-Str. 11, 12489 Berlin

knut.rurack@bam.de

### Supporting Information

S1. Literature overview .....	S-2
S2. Materials and methods.....	S-3
S3. Quantum chemical calculations, p <i>K</i> <sub>a</sub> correlation and prediction.....	S-6
S4. Smartphone software operation and algorithms.....	S-11
S5. Hardware development.....	S-21
S6. Absorption and emission spectra .....	S-23
S7. Reversibility .....	S-25
S8. Photophysics of <b>2</b> / <b>2H</b> <sup>+</sup> , <b>3</b> / <b>3H</b> <sup>+</sup> and <b>9</b> / <b>9</b> <sup>-</sup> .....	S-26
S9. Synthetic procedures .....	S-32
S10. References .....	S-44

## S1. Literature overview

**Table S1.** Representative literature on broad-range optical pH measurements with  $\Delta\text{pH} \geq 4$

pH range <sup>a</sup>	Device	System	reference
4–8	fluorometer	4 dyes in hydrogel matrix	1
4.5–8.5	fluorometer	1 dye grafted to hollow mesoporous silica nanoparticles	2
4.3–8.8	fiber-optic sensor (color)	3 dyes in sol-gel membrane	3
3.4–8.0	fluorometer	1 dye in polymerized micelles	4
0–5	fluorometer	1 polyprotic dye in solution	5
4–9	microfluidic sensor (color)	3 dyes in solution	6
5–10	fluorometer	QDs coated on dead bacterial spores	7
1.4–7.0	fluorometer	3 dyes in acrylamide nanoparticles	8
3.5–9	fluorometer	1 dye grafted to hollow mesoporous silica nanoparticles	9
3–9	sensor (luminescence)	Eu <sup>3+</sup> chelate-dye conjugate in FRET configuration	10
4–10	fluorometer	1 dye grafted to silica nanoparticles	11
0.5–7.0	fiber-optic sensor (color)	3 dyes in microspheres	12
2–9	fluorometer	4 dyes in hydrogel	13
1.5–9.0	fluorometer	2 dyes in acrylate membrane	14
1–9	fluorometer	amino-modified UiO-66-MOF	15
5–13	fluorometer	N-doped carbon dots in suspension	16
4.8–13	fluorometer	conjugated polymer-polyanion nanoparticle assembly	17
4.5–13	fiber-optic sensor (color)	3 dyes in sol-gel matrix	18
3–12	spectrophotometer	1 dye grafted to modified cellulose	19
5–14	fluorometer	1 dye, aggregate-induced emission in solution	20
–1–8.7	sensor (color)	2 dyes in polymer membrane	21
1–11	fluorometer	4 dyes in various membranes	22
1–14	fluorometer	7 dyes grafted to amino cellulose particles in hydrogel	23
0–14	scanner (color)	11 dyes in polyester membrane	24

<sup>a</sup> Ranges as given by the authors in the original articles.

## S2. Materials and methods

TLC experiments were performed on Merck Silica Gel 60 F<sub>254</sub> TLC plates. Reactions were monitored on TLC plates using a 254-nm hand-held UV lamp or stain solutions of KMnO<sub>4</sub>. Specifically, aldehydes were monitored using 2,4-dinitrophenylhydrazine stain solution. Column chromatography was carried out with Merck Silica gel 60 (0.040–0.063 mm) using dichloromethane (CH<sub>2</sub>Cl<sub>2</sub>) or petroleum ether:EtOAc as an eluent. NMR spectra were recorded on 400/500/600 MHz (100.6/125/151 MHz for <sup>13</sup>C) Bruker AV 400/500/600 spectrometers or on a 300 MHz (75.6 MHz for <sup>13</sup>C) Bruker DPX 300 spectrometer at 300 K using residual protonated solvent signals as internal standard (<sup>1</sup>H:  $\delta$  (CDCl<sub>3</sub>) = 7.26 ppm and <sup>13</sup>C:  $\delta$  (CDCl<sub>3</sub>) = 77.16 ppm). Assignments are based on chemical shifts and/or DEPT spectra. Mass spectra were measured on a Waters LCT Premier XE. UPLC was performed with a Waters UPLC Acquity equipped with a Waters LCT Premier XE mass detector for UPLC-MS, with Waters Alliance systems (consisting of a Waters Separations Module 2695, a Waters Diode Array detector 996 and a Waters Mass Detector ZQ 2000) equipped with a Acquity BEH C18 (2.1 × 50 mm) column, and with Shimadzu LC-10A systems equipped with a photodiode array detector (PAD). Fluorescence lifetimes were determined with a unique customized laser impulse fluorometer with picosecond time resolution described elsewhere.<sup>25,26</sup> The fluorescence lifetime profiles were analyzed with a PC using the software package FLA900 (Edinburgh Instruments).<sup>25,26</sup> Calibration of the pH meter was performed with standard aqueous solutions of pH 4.00, 7.00 and 9.00 from Metrohm GmbH. The measurement uncertainties of the pH electrodes amount to  $\leq \pm 0.03$  pH.

The following buffers were used: potassium chloride, phthalate, hydrogenphosphate, borate, carbonate and phosphate. Buffers were prepared according to ref. 27; Table S2 summarizes the details.

**Table S2.** Buffer compositions used, prepared according to 27.

pH	Component 1	Volume V <sub>1</sub> /mL	Component 2	Volume V <sub>2</sub> /mL	Vol. H <sub>2</sub> O /mL
0.51	KCl (0.2 M)	25.0	HCl (0.2 M)	67.0	100-(V <sub>1</sub> +V <sub>2</sub> )
1.23	KCl (0.2 M)	25.0	HCl (0.2 M)	20.7	100-(V <sub>1</sub> +V <sub>2</sub> )
2.02	KCl (0.2 M)	25.0	HCl (0.2 M)	6.5	100-(V <sub>1</sub> +V <sub>2</sub> )
2.51	Phthalate <sup>a</sup> (0.1 M)	50.0	HCl (0.1 M)	38.8	100-(V <sub>1</sub> +V <sub>2</sub> )
3.02	Phthalate <sup>a</sup> (0.1 M)	50.0	HCl (0.1 M)	22.3	100-(V <sub>1</sub> +V <sub>2</sub> )
3.54	Phthalate <sup>a</sup> (0.1 M)	50.0	HCl (0.1 M)	8.2	100-(V <sub>1</sub> +V <sub>2</sub> )
4.07	Phthalate <sup>a</sup> (0.1 M)	50.0	HCl (0.1 M)	0.1	100-(V <sub>1</sub> +V <sub>2</sub> )
4.58	Phthalate <sup>a</sup> (0.1 M)	50.0	NaOH (0.1 M)	8.7	100-(V <sub>1</sub> +V <sub>2</sub> )
5.08	Phthalate <sup>a</sup> (0.1 M)	50.0	NaOH (0.1 M)	22.6	100-(V <sub>1</sub> +V <sub>2</sub> )
5.58	Phthalate <sup>a</sup> (0.1 M)	50.0	NaOH (0.1 M)	36.6	100-(V <sub>1</sub> +V <sub>2</sub> )
6.08	KH <sub>2</sub> PO <sub>4</sub> (0.1 M)	50.0	NaOH (0.1 M)	5.6	100-(V <sub>1</sub> +V <sub>2</sub> )
6.49	KH <sub>2</sub> PO <sub>4</sub> (0.1 M)	50.0	NaOH (0.1 M)	13.9	100-(V <sub>1</sub> +V <sub>2</sub> )
7.01	KH <sub>2</sub> PO <sub>4</sub> (0.1 M)	50.0	NaOH (0.1 M)	29.1	100-(V <sub>1</sub> +V <sub>2</sub> )
7.52	KH <sub>2</sub> PO <sub>4</sub> (0.1 M)	50.0	NaOH (0.1 M)	41.1	100-(V <sub>1</sub> +V <sub>2</sub> )
7.98	KH <sub>2</sub> PO <sub>4</sub> (0.1 M)	50.0	NaOH (0.1 M)	46.7	100-(V <sub>1</sub> +V <sub>2</sub> )
8.49	Borate <sup>b</sup> (0.025 M)	50.0	HCl (0.1 M)	15.2	100-(V <sub>1</sub> +V <sub>2</sub> )
9.03	Borate <sup>b</sup> (0.025 M)	50.0	HCl (0.1 M)	4.6	100-(V <sub>1</sub> +V <sub>2</sub> )
9.57	Borate <sup>b</sup> (0.025 M)	50.0	NaOH (0.1 M)	8.8	100-(V <sub>1</sub> +V <sub>2</sub> )
9.89	NaHCO <sub>3</sub> (0.05 M)	50.0	NaOH (0.1 M)	10.7	100-(V <sub>1</sub> +V <sub>2</sub> )
10.20	NaHCO <sub>3</sub> (0.05 M)	50.0	NaOH (0.1 M)	17.8	100-(V <sub>1</sub> +V <sub>2</sub> )
10.87	NaHCO <sub>3</sub> (0.05 M)	50.0	NaOH (0.1 M)	22.7	100-(V <sub>1</sub> +V <sub>2</sub> )
11.76	Na <sub>2</sub> HPO <sub>4</sub> (0.05 M)	50.0	NaOH (0.1 M)	11.1	100-(V <sub>1</sub> +V <sub>2</sub> )
12.42	Na <sub>2</sub> HPO <sub>4</sub> (0.05 M)	50.0	NaOH (0.1 M)	26.9	100-(V <sub>1</sub> +V <sub>2</sub> )
12.95	KCl (0.2 M)	25.0	NaOH (0.2 M)	20.4	100-(V <sub>1</sub> +V <sub>2</sub> )
13.37	KCl (0.2 M)	25.0	NaOH (0.2 M)	66.0	100-(V <sub>1</sub> +V <sub>2</sub> )

*a*: KHC<sub>8</sub>H<sub>4</sub>O<sub>4</sub>. *b*: Na<sub>2</sub>B<sub>4</sub>O<sub>7</sub>·10 H<sub>2</sub>O.

For the measurement of whole pH range, the strip was first soaked in a solution buffered at  $\text{pH} \approx 7$  and allowed to equilibrate for 2 min. After that, the strip's signal was measured before repeating the procedure with the next pH solution in a decreasing order until the lower limit of the scale was reached. Afterwards, the strip was subjected to another soaking step at  $\text{pH} \approx 7$  before moving to the opposite pH limit. The temperature during the measurements was kept at  $24 \pm 1$  °C. The conditioning steps were made to minimize reproducibility errors due to drying of the hydrogel when storing the strips for different periods of time under normal laboratory conditions as well as to have the same reference point ( $\text{pH} \approx 7$ ) when recording titration curves. Long-term storage of the strips inside a buffered solution is not advised since the charged dye **R3** was found to show some leaching after one week.

### S3. Quantum chemical calculations, $pK_a$ correlation and prediction

The  $S_0$  ground-state geometries in the gas phase were optimized with the density functional theory (DFT) method employing the hybrid functional B3LYP with a 6-31G basis set and energy minimized as implemented in Gaussian 03.<sup>28</sup> As suggested by Seybold and co-workers,<sup>29</sup> Mulliken charges of the OH group in the phenol series ( $Q_{OH}$ ) and the amino substituent in the aniline series ( $Q_{An}$ ) were used for the correlation with the experimentally determined  $pK_a$  values.

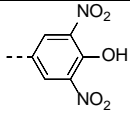
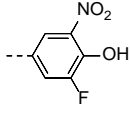
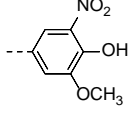
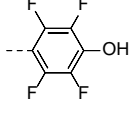
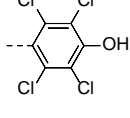
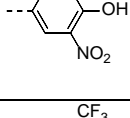
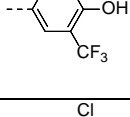
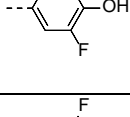
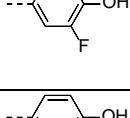
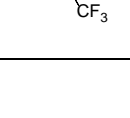
#### *S3.1 Phenol series.*

The iterative search for suitable proton-responsive phenol moieties was started with phenol, i.e., dye **9**, published by us earlier in 30, and dye **6**. After having established these two data points in the correlation, we screened first for other commercially available 4-hydroxybenzaldehyde derivatives, then calculated promising compounds and predicted their  $pK_a$ . In case the prediction was fitting into our scheme, we synthesized the respective compound and determined its  $pK_a$ . These results were then fed back into the correlation to improve the procedure. An iterative step-by-step procedure then yielded the library of phenols prepared. Various calculated structures were not realized synthetically, because their  $pK_a$  were predicted to be too close lying to already synthesized dyes. Some nitro-containing dyes, although showing very promising  $pK_a$ , could not be used in the sensor because their fluorescence was too weak even in the ON state. We always correlated both,  $Q_{OH}$  with experimental  $pK_a$  obtained in both EtOH:H<sub>2</sub>O 1:1 and the hydrogel. Table S3 gives an overview of the compounds considered and realized.

### S3.2 Aniline series.

The approach to aniline-type BODIPY pH indicators was very similar to the one described before for the phenols. Here, we had even more compounds available from earlier studies to set up the first correlation.<sup>31</sup> It turned out however that the correlation of calculated  $pK_a$  to those obtained in liquid solution (EtOH:H<sub>2</sub>O 1:1) was not promising. Although the hydrogel data showed a better correlation, it was still much less convincing than that of the phenol series. We assume that the interaction of the amino nitrogen's lone electron pair with potential hydrogen bond donors (solvent molecules, network molecules) as well as the degree of pyramidalization at the amino-N have a significant influence on the  $pK_a$ , potentially aggravating a simple correlation with atomic charges on the *meso*-group. The worse correlation compared with the phenol series led us to dispense with any more profound modeling and synthesis of predicted structures. Table S4 collects the relevant data.

**Table S3.** Calculated charges on the hydroxyl group and  $pK_a$  values (either measured or predicted) of the *meso*-phenol-BODIPYs considered here.<sup>a</sup>

<i>meso</i> -substituent	Abbreviation	$Q_{OH}$	$pK_a$ (EtOH:H <sub>2</sub> O)	$pK_a$ (hydrogel)
	–	–0.132	3.54 (pred.)	4.31 (pred.)
	–	–0.154	4.92 (pred.)	5.69 (pred.)
	<b>In7</b>	–0.161	6.09 (meas.)	7.05 (meas.)
	<b>4</b>	–0.181	5.13 (meas.)	6.11 (meas.)
	–	–0.184	6.90 (pred.)	7.67 (pred.)
	–	–0.188	6.41 (meas.)	7.41 (meas.)
	–	–0.190	7.29 (pred.)	8.07 (pred.)
	<b>6</b>	–0.194	8.91 (meas.)	9.53 (meas.)
	<b>5</b>	–0.195	7.40 (meas.)	8.43 (meas.)
	<b>7</b>	–0.214	8.75 (meas.)	9.96 (meas.)

<i>meso</i> -substituent	Abbreviation	$Q_{OH}$	$pK_a$ (EtOH:H <sub>2</sub> O)	$pK_a$ (hydrogel)
	–	–0.215	8.89 (pred.)	9.66 (pred.)
	–	–0.215	8.91 (pred.)	9.69 (pred.)
	–	–0.224	9.44 (pred.)	10.22 (pred.)
	<b>8</b>	–0.239	9.33 (meas.)	10.58 (meas.)
	–	–0.240	10.53 (pred.)	11.31 (pred.)
	<b>9</b>	–0.248	9.98 (meas.)	11.44 (meas.)
	<b>10</b>	–0.248	12.83 (meas.)	13.10 (meas.)

*a*: The correlations are as follows:  $y = -64,844x - 5.0496$  ( $r^2 = 0.7008$ ) for EtOH:H<sub>2</sub>O and  $y = -64,959x - 4.2958$  ( $r^2 = 0.8688$ ) for the hydrogel.

**Table S4.** Calculated charges on the amino group and  $pK_a$  values (either measured or predicted) of the *meso*-anilino-BODIPYs considered here.<sup>a</sup>

<i>meso</i> -substituent	Abbreviation	$Q_{OH}$	$pK_a$ (EtOH:H <sub>2</sub> O)	$pK_a$ (hydrogel)
	–	–0.117	0.0 (meas.)	not soluble
	–	–0.160	1.34 (meas.)	
	<b>In6</b>	–0.171	5.75 (meas.)	4.67 (meas.)
	<b>In3</b>	–0.180	2.87 (meas.)	2.11 (meas.)
	<b>In4</b>	–0.183	4.46 (meas.)	2.82 (meas.)
	–	–0.186	2.46 (meas.)	1.2 (meas.)
	<b>In2</b>	–0.187	1.55 (meas.)	0.95 (meas.)
	<b>3</b>	–0.200	4.62 (meas.)	3.29 (meas.)

<sup>a</sup>: The correlations are as follows:  $y = -0.0081x - 0.1498$  ( $r^2 = 0.3797$ ) for EtOH:H<sub>2</sub>O and  $y = -0.0153x - 0.1458$  ( $r^2 = 0.7688$ ) for the hydrogel.

## S4. Smartphone software operation and algorithms

Today, utmost smartphones and tablets still use the sRGB color space and produce non-RAW images that are gamma encoded; only some brand-new models also allow access to the RAW images, see also Section S4.5. To retrieve the desired luminance and hue values from the pictures recorded by the large majority of conventional smartphones like the one used here, linearization of the non-RAW image by reverting the gamma correction, yielding the RGB values, is necessary, before the image can then be transformed to any color space for further processing. Here, we transformed the RGB values to either the CIE XYZ or the HSB values (HSB = hue, saturation, brightness), because  $Y$  is equivalent to luminance (or fluorescence intensity), which we evaluated for dyes **3–10**, **R1** and **R2**, and  $H$  is hue which best correlates with the emission wavelength and was analyzed here for dyes **1**, **2**, **R1** and **R3**.

### S4.1 Obtaining luminance values

The RGB values for all pixels in each well, ranging from 0 to 255, are averaged to the arithmetic mean  $(\bar{R}, \bar{G}, \bar{B})$ , helping to reduce camera noise and any possible inhomogeneity in the sensing membrane. This is followed by a 0–1 normalization step.

These  $\overline{RGB}_0^1$  values are then transformed to the CIE 1931 XYZ color space, utilizing the standardized lineal transformation stated by the CIE (Commission internationale de l'éclairage) special commission<sup>32</sup> with a gamma correction factor of 2.2 and a D65 illuminant.

$$\begin{bmatrix} \bar{X} \\ \bar{Y} \\ \bar{Z} \end{bmatrix} = \begin{bmatrix} 0.412453 & 0.357580 & 0.180423 \\ 0.212671 & 0.715160 & 0.072169 \\ 0.019334 & 0.119193 & 0.950227 \end{bmatrix} \cdot \begin{bmatrix} \bar{R} & 1 \\ \bar{G} & 0 \\ \bar{B} & 0 \end{bmatrix} \quad (\text{S1})$$

#### S4.2 Obtaining Hue values

Hue is measured in degrees and its range is  $[0, 360]^\circ$ . Together with saturation ( $S$ , 0 to 1) and brightness ( $B$ , 0 to 1), these 3 values constitute the cylindrical *HSB* coordinate system. Conversion from *RGB* to *HSB* coordinate systems was performed by application of the original transformation (eq. S2).<sup>33</sup>

$$H = \begin{cases} 60^\circ \times \frac{G-B}{MAX-MIN} + 0^\circ, & \text{if } MAX = R \text{ and } G \geq B \\ 60^\circ \times \frac{G-B}{MAX-MIN} + 360^\circ, & \text{if } MAX = R \text{ and } G < B \\ 60^\circ \times \frac{G-B}{MAX-MIN} + 120^\circ, & \text{if } MAX = G \\ 60^\circ \times \frac{G-B}{MAX-MIN} + 240^\circ, & \text{if } MAX = B \end{cases} \quad (S2)$$

Applying the above formula to  $\overline{RGB}$ , we obtained the required  $\overline{H}$  value for the *meso*-pyridine dyes.

#### S4.3. Data mapping

$H$  or  $Y$  were the representative values ( $v_s^r$ ) for each of the 4-aminophenyl and 4-hydroxyphenyl or pyridin-4-yl dye derivatives, respectively.  $v_s^r$  was mapped for each sample with the corresponding representative values of its ON ( $v_{ON}^r$ ) and OFF ( $v_{OFF}^r$ ) references, according to eq. S3:

$$X_s = \frac{(v_s^r - v_{OFF}^r) \times c_s^{OFF}}{v_{ON}^r \times c_s^{ON}} \quad (S3)$$

Here,  $X_s$  is the fraction of the ON and OFF species of a sensor spot  $S$  as a function of the measured spectroscopic parameters of the sensor, ON and OFF references ( $v_s^r$ ,  $v_{ON}^r$ , and  $v_{OFF}^r$ , respectively) and the ON and OFF correction factors ( $c_s^{ON}$  and  $c_s^{OFF}$ ), respectively.

In this way, both the luminance  $Y$  or the hue  $H$  parameter were easily read through  $X_s$ , an indicative value of the fraction of the sensor  $s$  that is in an ON state.  $X_s$  ranges from 0 to 100, where 100 indicates that the sensor  $s$  is completely ON.

#### S4.4. Constraining and selecting useful data

Due to the sigmoidal dependence of the fluorescence of the probes on pH, the measurement of the pH value outside of the linear part of the curve can lead to an increased measurement error. A given pH is covered by the dynamic response range of (at best) three probes; all the others are either completely ON or OFF. Thus, it is necessary for the software to decide which probes are safe to be used for the measurement.

We achieved this by applying a threshold  $t$  to all the  $X_s$  values, considering for the next step those  $n$  values fulfilling the condition  $0 + t > X_s > 100 - t$ . In our experiments, we reached the best results with  $t = 10$ .

All values lying in the  $X_{st}^{100-t}$  range are considered as good values at first instance. An algorithm then checks if all the  $X_{st}^{100-t}$  values are corresponding to consecutive probes; in case a spot in either series shall be accidentally not fulfilling the criteria, presenting an outlier, it is ignored as being chemically not meaningful. Then, the software calculates the pH values for each of the  $X_{st}^{100-t}$  using the Henderson-Hasselbalch equation. It is assumed that both the  $Y$  and  $H$  parameter show a sigmoidal dependence with the pH.

$$pH = pKa + \log\left(\frac{A^-}{HA}\right) \quad (S4)$$

$$pH = pKa + \log\left(\frac{1-X_s}{X_s}\right) \times dx \quad (S5)$$

After averaging all the valid  $n$  values, a mean pH value ( $\overline{pH}$ ) with a standard deviation  $SD$  is obtained. In the extreme cases where all values are  $100-t < X_s$  or  $t > X_s$  (all probes lie outside of the linear range), the software will return the following pH values for such very basic or very acid situations, respectively:

$$pH > pKa_{10} + \log\left(\frac{t}{100-t}\right) \times dx_{10} \quad (S6)$$

$$pH < pKa_1 + \log\left(\frac{100-t}{t}\right) \times dx_1 \quad (S7)$$

#### S4.5. Calibration

Smartphone cameras that allow the manual adjustment of settings such as shutter speed and ISO, or provide images entirely in RAW format, are still rare,<sup>34</sup> even though Google Inc. has very recently published an API for interfacing cameras which allows executing such settings.<sup>35</sup>

Most of the present camera modules however auto-adjust the exposure time to achieve a better color distribution based on its internal histogram. For our application, this auto-adjustment has the drawback that it increases the very low luminance observed for the probes in their virtual OFF state, producing false luminance readings if not corrected. “Virtual OFF state” here means that the OFF state is never completely zero, but due to very small amounts of unavoidable background fluorescence always possesses a certain value. On the other hand, different exposure settings when all probes are ON, as well as subtle changes in environmental lighting, require the introduction of internal references for both the ON and OFF state. These internal reference dyes must be insensitive to pH changes so that the software can compare the luminance and normalize the luminance of every pH probe on these references.

It is thus necessary to know the luminance relation between each probe and the ON and OFF references ( $c_s^{ON}$  and  $c_s^{OFF}$ ). These correction factors need to be registered only once. Although they are currently still different for every strip, automated strip production should minimize this effort.

$$c_s^{OFF} = \frac{v_s^r}{v_{OFF}^r} \quad (S8)$$

$$c_s^{ON} = \frac{v_s^r - (v_{OFF}^r \times c_s^{OFF})}{v_{ON}^r} \quad (S9)$$

Thus, for obtaining the correction factors of a new strip, it must be introduced first into a strongly basic solution, and an image must be taken by pressing the *basic calibration* button in the *settings* drop-down menu of the application (Figure S1). Then these steps must be repeated with a strongly acid solution and the *acid calibration* button. After this two-point calibration, the software prompts for a file name so that the calibration parameters for that specific strip can be stored for further experiments. With these parameters, the fraction between the ON/OFF species of each sensor spot can be obtained with equation S3, see above.

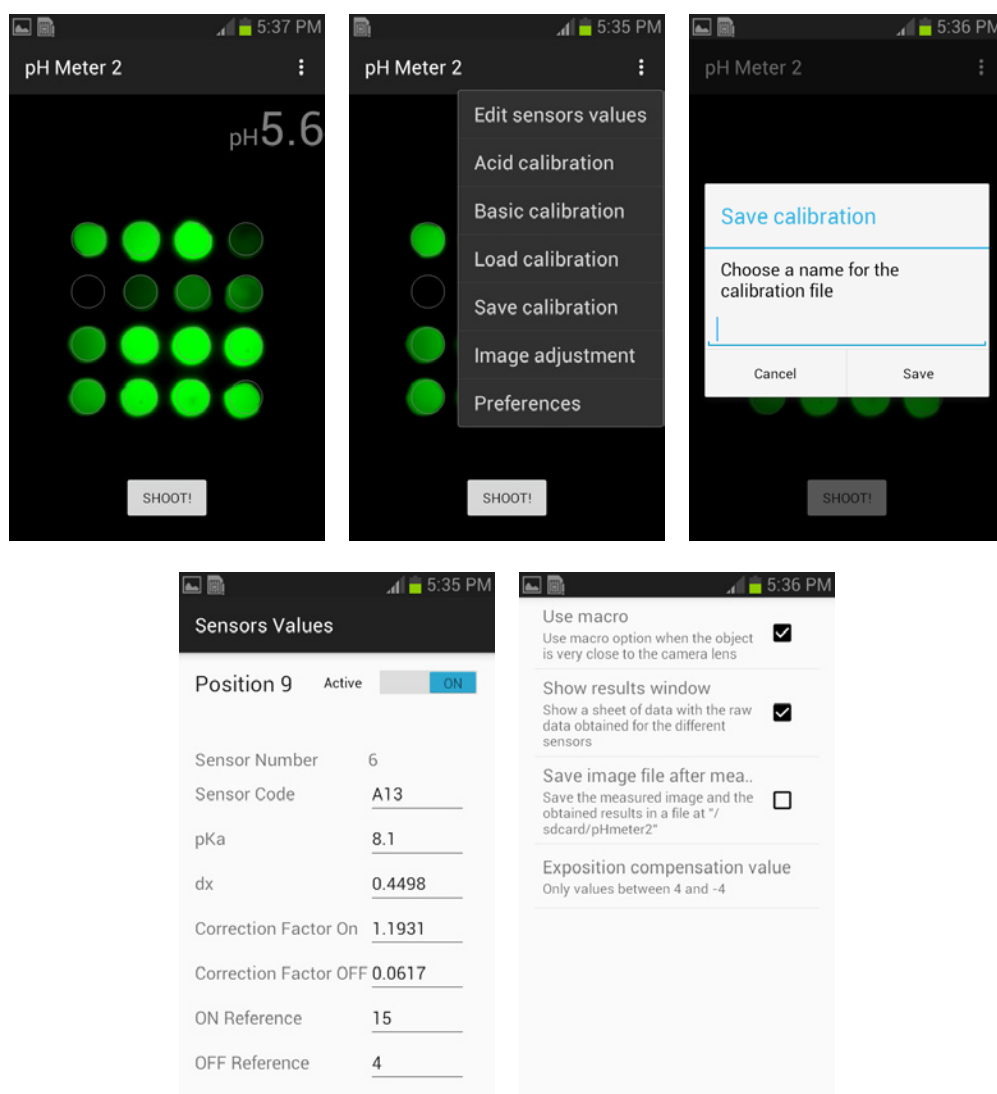


**Figure S1.** Screenshot of the written software for the measurement of the strips with the smartphone.

For better illustration, the procedure will be explained with the aid of an example. Figure S2 collects images shot with the smartphone devices of the same strip at pH 0.51, 13.37 and 11.76, extracted from a representative experiment.

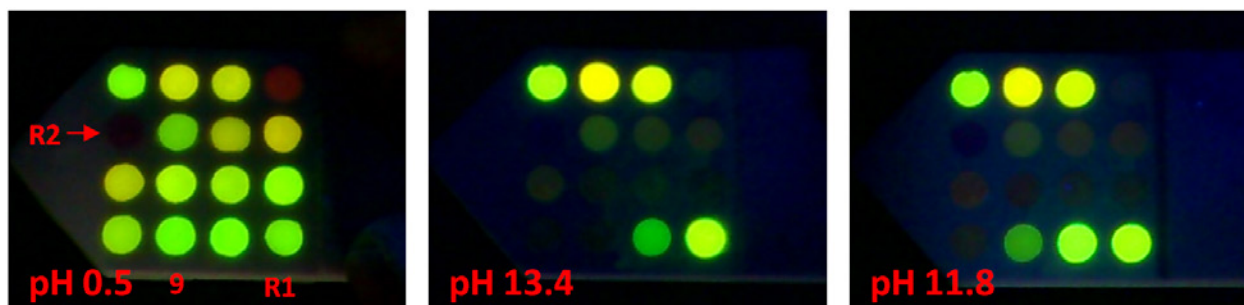


**Figure S2.** Smartphone pictures of the same strip at different pH values; a) pH 13.37, b) pH 0.51, and c) 11.76.

Pictures taken at pH 0.5 and pH 13.4 were used for calibration, because at pH 0.5 all amine- and pyridine-based dyes are protonated and the phenol-based dyes are in their neutral state. In contrast, at pH 13.4 the former two types of dyes are in their neutral state and the phenol-based dyes are deprotonated. In images a) and b) of Figure S2, dyes **R1** and **R2** are used to establish the correction factor between the different dyes and the references. In this example, the specific case of probe **9** will be considered.

Table S5 summarizes the luminance values obtained for dye **9** and references **R1** and **R2** at the different pH values. It is important to note how reference **R1**, which is constant during the whole experiment, shows higher luminance values when the strip was dipped into the solution at pH 13.4 than at pH 0.5. This is essentially due to the facts explained in Section S4.5. At pH 13.4, only few dyes are ON, so there is less light input at the CMOS. Then, the internal software of the camera triggers the auto-exposure compensation system to receive the stipulated average light that should be on a consumer picture. This results in a higher luminance for each spot. When all dyes are ON, i.e., at pH 0.5, there is more light reaching the CMOS and there is thus no need to set the

auto-exposure compensation to such a high gain. In contrast, it is adjusted until the average luminance of all the ON dyes reach the stipulated value. This variation would be a problem when attempting to measure the absolute value of a pH-sensitive dye such as **9**. However, if the constant internal references **R1** and **R2** are recorded, the luminance of **9** can be calculated relative to them. The detailed mathematical calibration procedure of the strip is shown in the following.

**Table S5.** Luminance values obtained by the smartphone for dye **9** and references **R1** and **R2** at different pH values

pH	Luminance values		
	Probe <b>9</b>	Reference <b>R1</b>	Reference <b>R2</b>
0.51	70.1	73.8	0.1
13.37	0.1	80.1	0.1
11.76	21.5	78.7	0.2

*Basic calibration step (OFF calibration):*

The strip is inserted into a basic solution (pH 13.37) and the image is recorded (Figure S2b), which yields the correction factor for the OFF state:

$$c_s^{OFF} = \frac{v_s^r}{v_{OFF}^r} \quad \text{where } v^r = \text{luminance}, s = \mathbf{9}, OFF = \mathbf{R2}$$

$$c_9^{OFF} = \frac{v_9^r}{v_{R2}^r} = \frac{0.1}{0.1} = 1.00$$

*Acidic calibration step (ON calibration):*

Next, the strip is inserted into an acidic solution (pH 0.51) and the image is recorded (Figure S2a), which yields the correction factor for the ON state:

$$c_s^{ON} = \frac{v_s^r - (v_{OFF}^r \times c_s^{OFF})}{v_{ON}^r} \quad \text{where } v^r = \text{luminance}, s = \mathbf{9}, OFF = \mathbf{R2}, ON = \mathbf{R1}$$

$$c_s^{ON} = \frac{v_9^r - (v_{R2}^r \times c_9^{OFF})}{v_{R1}^r} = \frac{70.1 - (0.1 \times 1)}{73.8} = 0.95$$

After the correction factors for the dyes have been obtained, the strip is fully calibrated and ready to measure a sample.

*Measurement of test sample:*

The strip is dipped into a test solution (pH 11.76). From Figure S2c we get:

$$X_s = \frac{(v_s^r - v_{OFF}^r \times c_s^{OFF})}{v_{ON}^r \times c_s^{ON}}$$

$$X_s = \frac{(v_9^r - v_{R2}^r \times c_9^{OFF})}{v_{R1}^r \times c_9^{ON}} = \frac{(21.5 - 0.2 \times 1)}{78.7 \times 0.95} = 0.28$$

Employing the Henderson-Hasselbalch equation, the pH according to probe **9** can be calculated:

$$pH = pKa + \log\left(\frac{1-X_s}{X_s}\right) \times dx = 11.49 + \log\left(\frac{1-0.28}{0.28}\right) \times 0.344 = 11.63.$$

#### S4.6 Fine tuning of $pK_a$ values

During our studies, we observed minor deviations between the  $pK_a$  values measured with the fluorometer and those obtained with the smartphone system. These deviations were constant across different strips. We attributed these differences to the slightly different composition of the hydrogel matrix used in the wells with respect to the hydrogel coated onto slides that were used for the fluorometer experiments (Table S6).

**Table S6.** Measured  $pK_a$  values for the dyes **1–10** in two different hydrogel matrix compositions.

Matrix composition (D4 : EtOH : H <sub>2</sub> O, w / w / w)	<b>1</b>	<b>2</b>	<b>3</b>	<b>4</b>	<b>5</b>	<b>6</b>	<b>7</b>	<b>8</b>	<b>9</b>	<b>10</b>
0.09 : 0.11 : 1	0.50	2.34	3.29	6.11	8.43	8.94	9.96	10.58	11.44	12.83
0.18 : 0.11 : 1	0.50	1.48	2.92	5.20	8.1	7.56	9.54	10.15	11.49	13.09
$\Delta pK_a$	0.00	0.86	0.37	0.99	0.33	1.38	0.42	0.43	0.05	0.26

In fact, the activity of protons is higher in hydrogels with a higher water content, arriving at  $\Delta pK_a$  between diluted and concentrated hydrogel matrix which should be considered. Because the hydrogel matrix used for the strip arrays was too viscous to prepare dip coated strips for measurement in the fluorometer, the  $pK_a$  data had to be determined again with the final strip test.

Using the previously described UV-cabinet setup, we recorded pictures of the strips at different pH. Then we were able to measure the fluorescence intensity changes of all the different dyes in terms of luminance or hue accordingly using a custom software tool in a desk computer. The obtained values were independently plotted versus the measured pH. Fitting of these values yielded the theoretical curves for the titration profiles.

### S4.7 pH coverage of strips

Making use of the latest measured  $pK_a$  values we could determine the response of each sensor in the strip against the pH (Figure S3).

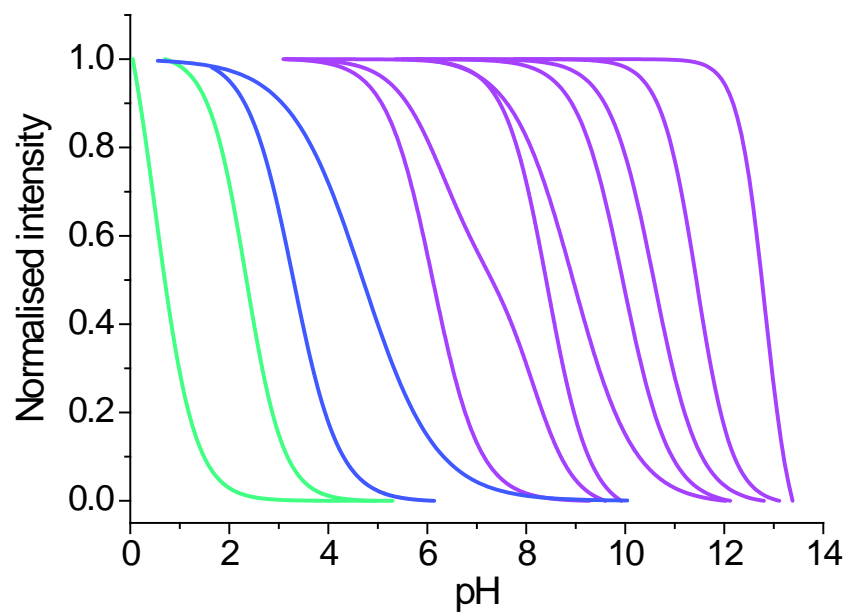


**Figure S3.** Normalized titration profiles (fluorescence intensity  $I_F$  at maximum  $\lambda_{em}$  vs pH) of the pH-sensors (from left to right) **1, 2, 3, 3+4, 4, 4+5, 5, 6, 7, 8, 9** and **10** in the D4 Hydrogel matrix. Profiles for **1** and **2** are shown inverted ( $1-I_F$ ) for better clarity.

## S5. Hardware development

### S5.1 Smartphone adaption of optical system and case design

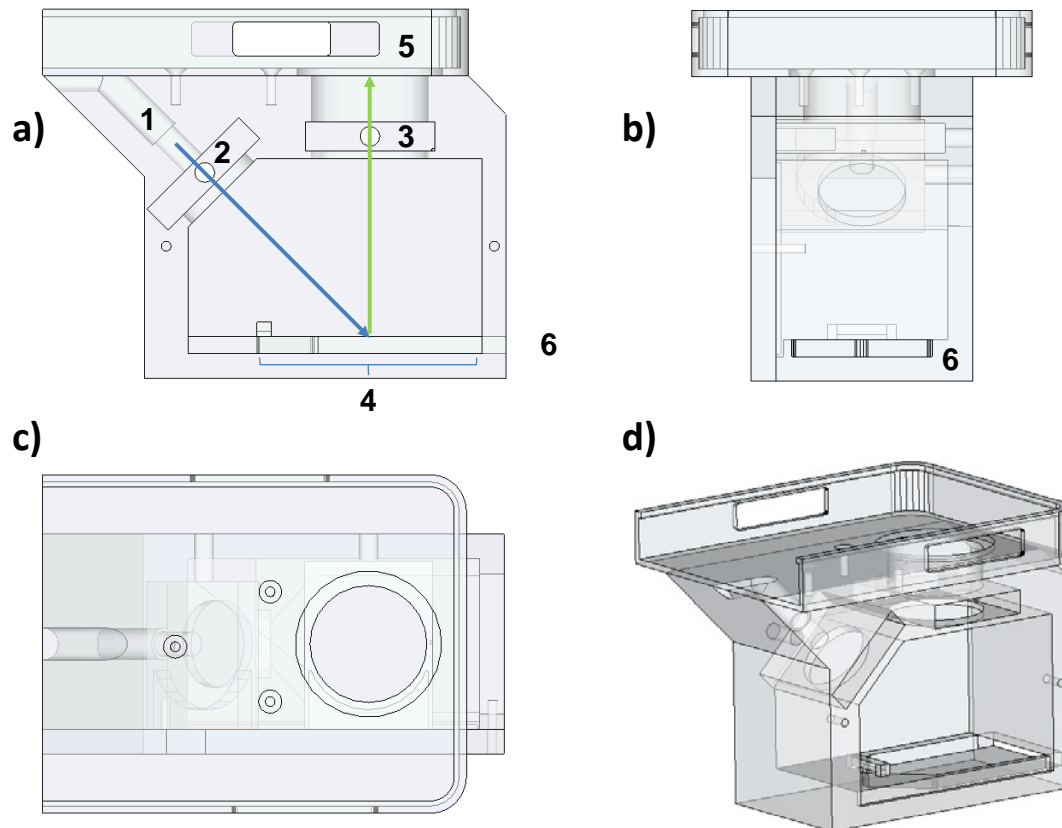


**Figure S4.** Schematic representation of the smartphone adapter including sample mount and case: a) side, b) front, c) top and d) free view. Numbers in view a) stand for 1) accommodation for light source, accommodation for 2) excitation and 3) emission filters, 4) position of the strip to be measured, 5) position of the smartphone CMOS, 6) slot for strip insertion.

## S5.2 Matching of optical components

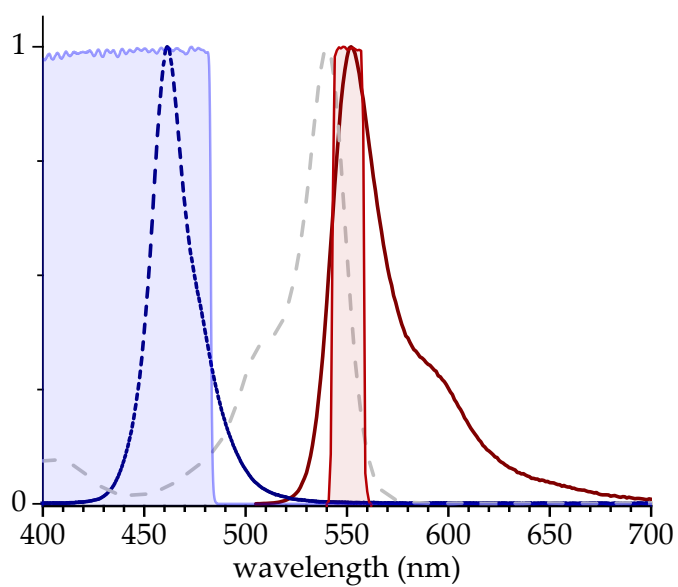


**Figure S5.** Emission spectrum of Blau Nichia LED (model NSPB500AS, 11000 mcd, 15°) (blue line), absorption (grey line) and emission (red line) spectra of **3** as well as transmission characteristics of short-pass (light blue area) and band-pass (light red area) filters. All spectra are normalized for better comprehension.

## S6. Absorption and emission spectra

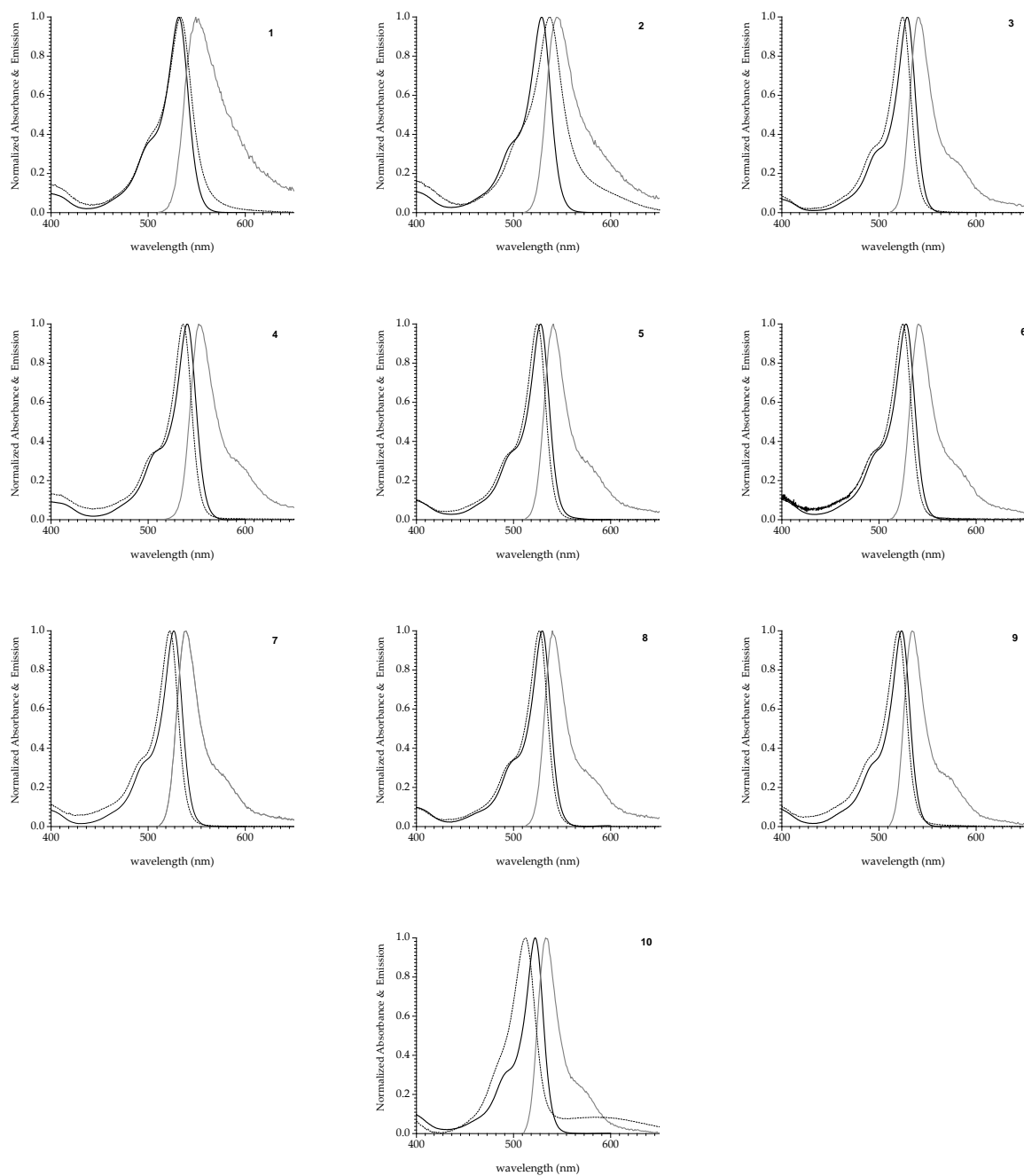


**Figure S6.** Normalized absorption and emission spectra of dyes **1–10** *c.a.*  $10^{-6}$  M in EtOH:H<sub>2</sub>O 1:1 mixtures. Solid (—) and dashed (---) lines indicate ON and OFF states respectively.

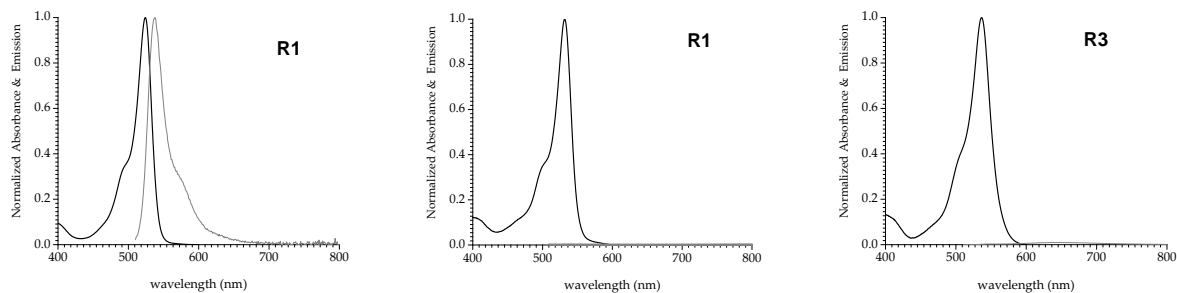


**Figure S7.** Normalized absorption and emission spectra of reference dyes **R1**, **R2** and **R3** *ca.*  $10^{-6}$  M in EtOH:H<sub>2</sub>O 1:1 mixtures. Emission spectra of **R2** and **R3** are relative to **R1**.

**Table S7.** Fluorescence lifetimes of selected probes in the ON and OFF states in H<sub>2</sub>O:EtOH 1:1 (v/v).

Cmpd.	State	$\tau_f$ /ns
<b>3</b>	ON	5.36
<b>4</b>	ON	6.74
<b>5</b>	ON	5.43
<b>6</b>	ON	5.91
<b>7</b>	ON	5.70
<b>8</b>	ON	6.26
<b>9</b>	ON	5.57

Cmpd.	State	$\tau_f$ /ns
<b>10</b>	ON	5.64
<b>In2</b>	ON	5.80
<b>In3</b>	ON	5.40
<b>In4</b>	ON	5.00
<b>In5</b>	ON	5.07
<b>In6</b>	ON	5.78
<b>In6</b>	OFF	1.17

## S7. Reversibility

To check the reversibility of the system, strips were exposed to intense pH changes during at least 10 cycles going from pH 2.51 to pH 10.20. Apart from a slight deviation from the values determined with the pH electrode,  $\text{pH } 2.58 \pm 0.17$  and  $\text{pH } 10.32 \pm 0.22$ , no trends in the pH values or the precision of the measurement were observed, indicating that the sensor is reversible and stable for these pH changes (Figure S8).

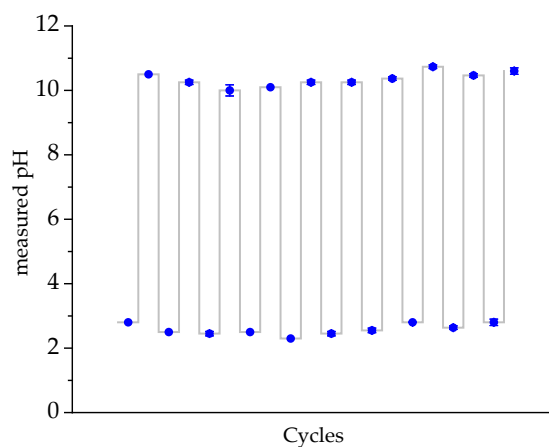


**Figure S8.** Representative train of pH values obtained during 10 cycles of soaking the strip alternately in solutions of pH 2.51 and pH 10.20 for 17 min.

## S8. Photophysics of **2** / **2H<sup>+</sup>**, **3** / **3H<sup>+</sup>** and **9** / **9<sup>-</sup>**

**Table S8.** Calculated properties for the vertical excitation of the energy-minimized ground-state geometries of **2** / **2H<sup>+</sup>**, **3** / **3H<sup>+</sup>** and **9** / **9H<sup>+</sup>**.

	$\lambda_{S_n \leftarrow S_0}^{(n)}$ /nm [a]	$f$ [b]	$\Delta\mu_{S_n-S_0}$ /D [c]	Orbitals (coefficients) [d]
<b>2</b>	432.0 (1)	<b>0.419</b>	-2.0	HOMO-LUMO (0.53), HOMO-1-LUMO (0.29)
	372.6 (2)	0.262	0.0	HOMO-LUMO (-0.30), HOMO-1-LUMO (0.64)
	359.1 (3)	0.039	-1.0	HOMO-2-LUMO (0.70)
	339.2 (4)	0.001	<b>15.4</b>	HOMO-LUMO+1 (0.70)
	317.9 (5)	0.000	<b>25.0</b>	HOMO-3-LUMO (0.71)
<b>2H<sup>+</sup></b>	2269.1 (1)	0.000	-16.9	HOMO-LUMO (0.7)
	741.0 (2)	0.013	-17.2	HOMO-LUMO+1 (0.7)
	719.2 (3)	0.000	-18.7	HOMO-1-LUMO (0.71)
	677.9 (4)	0.000	-18.8	HOMO-2-LUMO (0.71)
	441.0 (5)	0.192	-18.2	HOMO-1-LUMO+1 (0.70)
	440.2 (6)	<b>0.386</b>	-5.9	HOMO-LUMO+2 (0.50), HOMO-1-LUMO+2 (-0.18), HOMO-2-LUMO+1 (0.33)
	422.7 (7)	0.136	-15.0	HOMO-LUMO+2 (-0.30), HOMO-1-LUMO+2 (0.15), HOMO-2-LUMO+1 (0.62)
<b>3</b>	546.9 (1)	0.000	<b>23.6</b>	HOMO-LUMO (0.70)
	429.0 (2)	<b>0.425</b>	-2.5	HOMO-1-LUMO (0.56), HOMO-2-LUMO (0.25)
	375.5 (3)	0.146	3.4	HOMO-1-LUMO (-0.24), HOMO-2-LUMO (0.66) HOMO-4-LUMO (-0.10)
	353.8 (4)	0.042	-1.1	HOMO-3-LUMO (0.70)
	339.0 (5)	0.059	<b>14.9</b>	HOMO-1-LUMO (-0.11), HOMO-4-LUMO (0.69)

	$\lambda_{s_n \leftarrow s_0}^{(n)}$ /nm [a]	$f$ [b]	$\Delta\mu_{s_n-s_0}$ /D [c]	Orbitals (coefficients) [d]
<b>3H<sup>+</sup></b>	449.0 (1)	0.016	-20.9	HOMO-LUMO (-0.14), HOMO-LUMO+1 (0.69)
	440.8 (2)	<b>0.399</b>	-3.0	HOMO-LUMO (0.53), HOMO-LUMO+1 (0.15), HOMO-1-LUMO (-0.27)
	393.3 (3)	0.000	-20.7	HOMO-LUMO+2 (0.70)
	377.0 (4)	0.219	-0.1	HOMO-LUMO (0.28), HOMO-1-LUMO (0.65)
	364.8 (5)	0.039	-1.0	HOMO-2-LUMO
<b>9</b>	430.0 (1)	<b>0.427</b>	-1.6	HOMO-LUMO (0.54), HOMO-1-LUMO (0.29)
	370.8 (2)	0.250	0.1	HOMO-LUMO (-0.22), HOMO-1-LUMO (0.60)
	366.7 (3)	0.005	<b>19.6</b>	HOMO-2-LUMO (0.47), HOMO-3-LUMO (0.52)
	356.2 (4)	0.038	-0.8	HOMO-2-LUMO (0.49), HOMO-3-LUMO (-0.45)
	298.3 (5)	0.005	9.9	HOMO-LUMO+1 (0.7)
<b>9<sup>-</sup></b>	5216.0 (1)	0.000	-3.4	HOMO-LUMO (0.7)
	1205.4 (2)	0.001	4.5	HOMO-1-LUMO (0.7)
	489.0 (3)	0.000	-7.7	HOMO-2-LUMO (0.11), HOMO-3-LUMO (0.69)
	414.6 (4)	<b>0.456</b>	1.9	HOMO-2-LUMO (0.55), HOMO-4-LUMO (0.26)
	358.2 (5)	0.192	-0.2	HOMO-2-LUMO (-0.20), HOMO-4-LUMO (0.62)

[a] Wavelength of the transition. [b] Oscillator strength of the transition. [c] Dipole moment difference between ground ( $\mu_0$ ) and respective excited ( $\mu_n$ ) state. [d] MOs involved in the transitions.

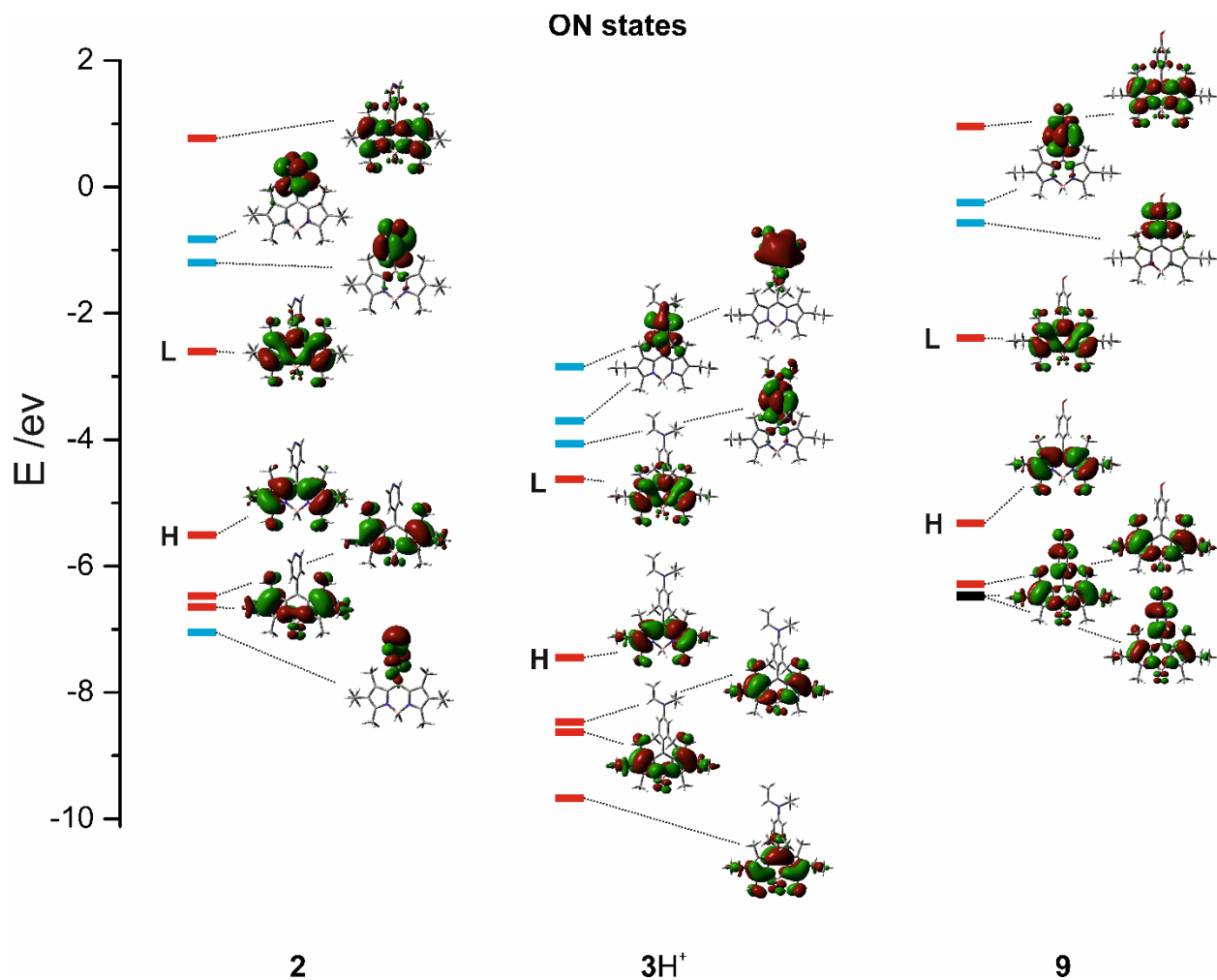


**Figure S9.** Frontier molecular orbitals of geometry-optimized ON states of **2**, **3** and **9**, neutral **2** and **9** and protonated **3H<sup>+</sup>**; HOMO and LUMO are denoted by “H” and “L”, BODIPY-localized MOs in red, *meso*-substituent-localized MOs in blue, MOs localized on both fragments in black.

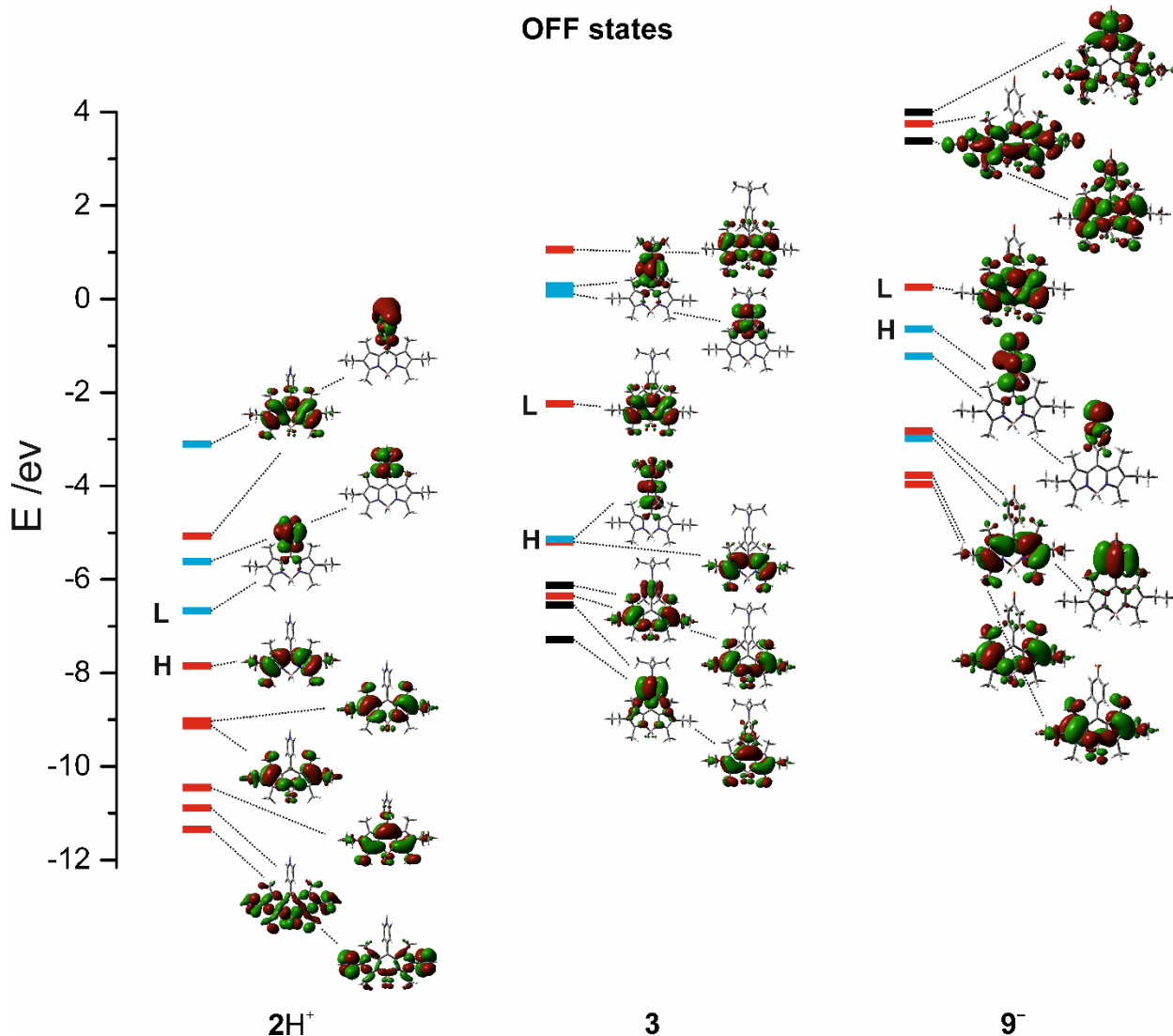


**Figure S10.** Frontier molecular orbitals of geometry-optimized OFF states of **2**, **3** and **9**, protonated **2H<sup>+</sup>**, neutral **3** and deprotonated **9<sup>-</sup>**; HOMO and LUMO are denoted by “H” and “L”, BODIPY-localized MOs in red, *meso*-substituent-localized MOs in blue, MOs localized on both fragments in black.

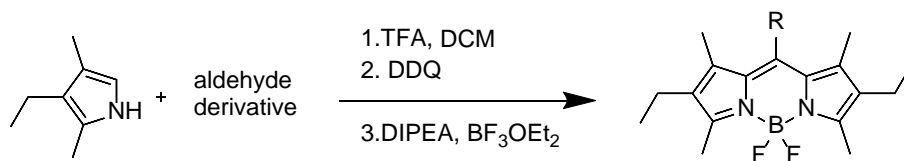
Quantum chemical calculations were carried out to better illustrate the photophysical process active in the probes developed here. Optimization of the  $S_0$  ground state geometries in the gas phase was performed with the density functional theory (DFT) method employing the hybrid functional B3LYP with a 6-31G basis set and energy-minimized as implemented in Gaussian 09.<sup>36</sup>

Figures S9 and S10 collect the frontier molecular orbitals of the ON and OFF states of three representative probes of *meso*-pyridine (**2**), aniline (**3**) and phenol type. Table S8 contains the calculated properties for the vertical excitation of the energy-minimized ground-state geometries.

Table S8 shows that for the neutral ON states **2** and **9** the lowest oscillator-strong transition is found at ca. 430 nm in the gas phase, followed by a weaker transition at ca. 370 nm and several distinctly weaker transitions up to ca. 300 nm (the next oscillator-strong transitions are only centred at ca. 260 nm). In case of **2**, the strongly forbidden and highly dipolar charge-transfer states  $S_4$  and  $S_5$  are too high lying in energy (93 nm or 0.8 eV as well as 114 nm or 1 eV) so that even in a polar solvent environment they are not sufficiently stabilized to become  $S_1$ . For  $3H^+$ , the situation is qualitatively similar. Although the lowest oscillator-strong transition is somewhat red-shifted (440 nm), which is in line with the well-known protonation-induced absorption shifts of *meso*-aniline BODIPYs, see also Figure S6, the next transitions are all oscillator-weak like for **2** and **9**. Moreover, although this transition is only the  $S_2$  state for  $3H^+$ , the mixed and oscillator-weaker  $S_1$  state is only 0.05 eV (or 8 nm) lower lying in energy so that, due to the much higher negative dipole moment of the  $S_1$  compared with the  $S_2$  state,  $S_1$  is strongly destabilized in a highly polar solvent environment and, hence,  $S_1$  and  $S_2$  state change order;  $3H^+$  approximates **2** and **9**, and for all the oscillator-strong transitions of the three dyes, the corresponding triplet states are shifted by  $\geq 1.4$  eV, precluding any quenching influence via that route. The similarity of the three ON states is well-reflected by the molecular orbitals shown in Figure S9. Both HOMO and LUMO are localized on the same molecular fragment and any perturbation is unlikely to happen because MOs localized on the *meso*-substituent are either much lower lying (occupied MOs) or higher lying (unoccupied MOs), the latter being not significantly involved in the  $S_1$  to  $S_5$  transitions.

The situation is different for the OFF states, see Table S8 and Figure S10. Especially Figure S10 nicely shows that for all the three OFF states **2H<sup>+</sup>**, **3** and **9<sup>-</sup>**, HOMO and LUMO are now localized exactly on opposite fragments of the probe molecule, which are decoupled due to the perpendicular orientation (interannular twisting angles were calculated to lie between 89° and 90°). The HOMO–LUMO transition is in all three cases thus strongly forbidden. A look at Table S8 confirms this: for all three probes, the HOMO–LUMO transition is connected to  $f = 0$ . Since this transition is also the S<sub>1</sub> state in all three molecules, weak or no emission is to be expected. This transition is extremely low-lying in the two charged species, **2H<sup>+</sup>** and **9<sup>-</sup>**, and still 0.6 eV (or 118 nm) energetically favored in **3**. Since this state is additionally connected to a much higher dipole moment (23.6 D) than the next, BODIPY-centered S<sub>2</sub> state at 429 nm (–2.5 D), it is still stronger stabilized in a polar solvent environment, reinforcing the trend. Figure S10 nicely shows that there is at least one *meso*-group-centered MO lying between the BODIPY-centered MOs, potentially acting as an electron donating or accepting partner in a photoinduced electron-transfer type quenching process. As above for the ON states, all three OFF states thus show a qualitatively similar behavior. Moreover, as would be expected for such decoupled structures, singlet-triplet energy differences are very small with  $\Delta E_{S-T} \approx 0.01$  eV for the S<sub>1</sub>/T<sub>1</sub> pairs. Efficient non-radiative deactivation is thus expected. In agreement with the solution data, the first transitions of sizeable oscillator strength are found at 440 nm for **2H<sup>+</sup>**, 429 nm for **3** and 415 nm for **9<sup>-</sup>**, i.e., slightly bathochromically (for **2H<sup>+</sup>**) or hypsochromically shifted (**3**, **9<sup>-</sup>**) compared to **2** as well as **3H<sup>+</sup>** and **9**. These features again reflect the general BODIPY behavior well, i.e., a positive inductive effect (+I effect) at the *meso*-C atom leads to red-shifted, a –I effect to blue-shifted spectra.

## S9. Synthetic procedures



**General procedure for the synthesis of BOPDIPYs.** To a solution of 2.3 eq. of 3-ethyl-2,4-dimethylpyrrole in dry CH<sub>2</sub>Cl<sub>2</sub>, 1 eq. of the appropriate benzaldehyde was added followed by a catalytic amount of trifluoroacetic acid (TFA). After the resulting reddish solution stirring overnight, 1.3 eq. of 2,3-dichloro-5,6-dicyanobenzoquinone (DDQ) were added and the mixture was stirred for an additional 1 h. If TLC analysis (4:1 PE:EtOAc + 1% Et<sub>3</sub>N) revealed incomplete oxidation, another 0.5 eq. of DDQ were added. All reactions were complete after 2 h. Subsequently, 7 eq. of *N,N*-diisopropylethylamine (DIPEA) and BF<sub>3</sub>·OEt<sub>2</sub> were added. After 1 h, the mixture was concentrated in vacuo, re-dissolved in EtOAc and washed with water. The water layer was extracted with EtOAc and the combined organic layers were dried with Na<sub>2</sub>SO<sub>4</sub>, filtered and concentrated under reduced pressure. The products were purified with column chromatography.

**Dye R1. 8-(phenyl)-1,3,5,7-tetramethyl-2,6-diethyl-4,4-difluoro-4-bora-3a,4a-diaza-s-indacene.** The synthetic procedure was adopted from ref. 37. The crude product was purified by column chromatography on silica using toluene as eluent to give compound **R1** as bright reddish crystals (441 mg, 29%). <sup>1</sup>H-NMR (500 MHz, CDCl<sub>3</sub>) δ 0.98 (t, 6H, *J* = 7.6 Hz), 1.27 (s, 6H), 2.29 (q, 4H, *J* = 7.6 Hz), 2.53 (s, 6H), 7.27-7.29 (m, 2H), 7.46-7.48 (m, 3H) ppm. HR-MS (ESI<sup>+</sup>): *m/z* calculated for C<sub>23</sub>H<sub>28</sub>BF<sub>2</sub>N<sub>2</sub> [M+H]<sup>+</sup>: 381.2314, found: 381.2267.

**Dye R2. 8-(4-(dimethylamino)-2-nitrophenyl)-1,3,5,7-tetramethyl-2,6-diethyl-4,4-difluoro-4-bora-3a,4a-diaza-s-indacene.** **R2** was synthesized following the general procedure using 500 mg (2.53 mmol) of 5-nitrovanillin and purified using silica column chromatography

using DCM:PE (64:36) as eluent. 234 mg, 19 % Yield.  $^1\text{H-NMR}$  (600 MHz DMSO- $d_6$ )  $\delta$  = 7.38 (dd, 1H,  $J$  = 8.7, 2.7 Hz), 7.28 (d, 1H,  $J$  = 8.6 Hz), 7.17 (dd, 1H,  $J$  = 8.7, 2.7 Hz), 3.07 (s, 6H), 2.43 (s, 6H), 2.29 (q, 4H,  $J$  = 7.6 Hz), 1.35 (s, 6H), 0.94 (t, 6H,  $J$  = 7.6 Hz).  $^{13}\text{C-NMR}$  (150 MHz DMSO- $d_6$ )  $\delta$  153.0, 150.9, 148.9, 137.1, 136.6, 132.4, 131.0, 130.2, 116.8, 114.6, 106.0, 40.0, 16.3, 14.4, 12.2, 10.8 ppm. HR-MS (ESI+):  $m/z$  calculated for  $\text{C}_{25}\text{H}_{32}\text{BF}_2\text{N}_4\text{O}_2$   $[\text{M}+\text{H}]^+$ : 469.2586, found: 469.2566.

**Dye R3. 4-(1,3,5,7-tetramethyl-2,6-diethyl-4,4-difluoro-4-bora-3a,4a-diaza-s-indacen-8-yl)-1-methylpyridinium.** Dye 2 (0.1 mmol, 38 mg) and methyl iodide (1.0 mmol, 67  $\mu\text{L}$ ) were dissolved in 10 mL toluene. Then, the mixture was refluxed for 5 h. After that time, the solvent was evaporated, and the mixture was purified using silica column chromatography using DCM:MeOH (9:1 v/v) as eluent. 23 mg, yield 44%.  $^1\text{H NMR}$  (600 MHz, Chloroform- $d$ )  $\delta$  9.59 – 9.54 (m, 2H), 8.02 – 7.98 (m, 2H), 4.90 (s, 3H), 2.53 (s, 6H), 2.29 (q,  $J$  = 7.5 Hz, 4H), 1.39 (s, 6H), 0.97 (t,  $J$  = 7.5 Hz, 6H).  $^{13}\text{C NMR}$  (151 MHz,  $\text{CDCl}_3$ )  $\delta$  156.91, 154.35, 146.34, 137.02, 134.61, 130.85, 128.68, 128.47, 50.36, 17.03, 14.48, 13.75, 12.77. HR-MS (ESI+):  $m/z$  calculated for  $\text{C}_{23}\text{H}_{29}\text{BF}_2\text{N}_3$   $[\text{M}-\text{I}]^+$ : 396.2426, found: 396.2428.

**Dye 1. 8-(2-chloropyridin-4-yl)-1,3,5,7-tetramethyl-2,6-diethyl-4,4-difluoro-4-bora-3a,4a-diaza-s-indacene. 1** was synthesized following the general procedure using 516 mg (3.64 mmol) of 2-chloro-4-pyridinecarboxyaldehyde and purified using silica column chromatography using DCM:PE (81:19) as eluent. 526 mg, 35 % Yield.  $^1\text{H-NMR}$  (400 MHz DMSO- $d_6$ )  $\delta$  = 8.61 (d, 1H,  $J$  = 5.0 Hz), 7.78 (s, 1H), 7.56 (dd, 1H,  $J$  = 5.0, 1.2 Hz), 2.43 (s, 6H), 2.29 (q, 4H,  $J$  = 7.5 Hz), 1.32 (s, 6H), 0.93 (t, 6H,  $J$  = 7.5 Hz) ppm.  $^{13}\text{C-NMR}$  (100 MHz DMSO- $d_6$ )  $\delta$  154.4, 151.3, 151.0, 146.5, 137.6, 135.2, 133.3, 128.8, 124.1, 123.2, 16.4, 14.5, 12.3, 11.7, ppm. HR-MS (ESI+):  $m/z$  calculated for  $\text{C}_{22}\text{H}_{26}\text{BF}_2\text{N}_3\text{Cl}$   $[\text{M}+\text{H}]^+$ : 416.1876, found: 416.0285.

**Dye 2. 8-(pyridin-4-yl)-1,3,5,7-tetramethyl-2,6-diethyl-4,4-difluoro-4-bora-3a,4a-diaza-s-indacene. 2** was synthesized following the general procedure with 500 mg (5.31 mmol) of 4-pyridinecarboxyaldehyde.  $\text{CH}_2\text{Cl}_2$  was used in the work-up. Purification was done via silica column chromatography using DCM:EtOAc (95:5) as eluent. 614 mg, 30 % Yield.  $^1\text{H-NMR}$  (400 MHz DMSO- $d_6$ )  $\delta$  = 8.76 (d, 2H,  $J$  = 4.3 Hz), 7.48 (d, 2H,  $J$  = 4.9 Hz), 2.43 (s, 6H), 2.28 (q, 4H,  $J$  = 7.6 Hz), 1.27 (s, 6H), 0.93 (t, 6H,  $J$  = 7.5 Hz) ppm.  $^{13}\text{C-NMR}$  (100 MHz DMSO- $d_6$ )  $\delta$  154.0, 150.5, 142.9, 137.8, 137.0, 133.1, 129.0, 123.5, 16.4, 14.5, 12.3, 11.5 ppm. HR-MS (ESI+):  $m/z$  calculated for  $\text{C}_{22}\text{H}_{27}\text{BF}_2\text{N}_3$   $[\text{M}+\text{H}]^+$ : 382.2266, found: 382.2057.

**Dye 3. 8-(4-(diethylamino)-2,6-dimethylphenyl)-1,3,5,7-tetramethyl-2,6-diethyl-4,4-difluoro-4-bora-3a,4a-diaza-s-indacene. 3** was synthesized following the general procedure with 185 mg (0.901 mmol) of **A6**.  $\text{CH}_2\text{Cl}_2$  was used in the work-up. Purification was done via silica column chromatography using DCM as eluent. 126 mg, 29 % yield.  $^1\text{H-NMR}$  (600 MHz DMSO- $d_6$ )  $\delta$  = 6.52 (s, 1H), 3.33 (q, 4H,  $J$  = 7.1 Hz), 2.42 (s, 6H), 2.29 (q, 4H,  $J$  = 7.6 Hz), 1.95 (s, 6H), 1.36 (s, 6H), 1.10 (t, 6H,  $J$  = 7.0 Hz), 0.95 (t, 6H,  $J$  = 7.5 Hz).  $^{13}\text{C-NMR}$  (150 MHz DMSO- $d_6$ )  $\delta$

152.2, 147.7, 140.9, 137.5, 134.9, 131.9, 130.0, 120.7, 111.0, 43.3, 19.7, 16.4, 14.5, 12.2, 12.1, 10.1 ppm. HR-MS (ESI+):  $m/z$  calculated for  $C_{29}H_{41}BF_2N_3$   $[M+H]^+$ : 480.3362, found: 480.2785.

**Dye 4. 8-(4-hydroxy-2,3,5,6-tetrafluorophenyl)-1,3,5,7-tetramethyl-2,6-diethyl-4,4-difluoro-4-bora-3a,4a-diaza-s-indacene.** **4** was synthesized following the general procedure using 600 mg (3.09 mmol) of 4-hydroxy-1,2,3,4-tetrafluorobenzaldehyde and purified using silica column chromatography using EtOAc:PE (50:50) as eluent. 416 mg, 29 % Yield.  $^1H$ -NMR (400 MHz DMSO- $d_6$ )  $\delta$  = 12.23 (s, 1H), 2.45 (s, 6H), 2.33 (q, 4H,  $J$  = 7.6 Hz), 1.53 (s, 6H), 0.97 (t, 6H,  $J$  = 7.6 Hz).  $^{13}C$ -NMR (100 MHz DMSO- $d_6$ )  $\delta$  155.2, 144.1, 145.6, 139.4, 137.1, 133.5, 130.0, 122.6, 101.8, 16.3, 14.3, 12.3, 10.3. ppm. HR-MS (ESI+):  $m/z$  calculated for  $C_{23}H_{24}BF_6N_2O$   $[M+H]^+$ : 469.1886, found: 469.1899.

**Dye 5. 8-(3,5-difluoro-4-hydroxyphenyl)-1,3,5,7-tetramethyl-2,6-diethyl-4,4-difluoro-4-bora-3a,4a-diaza-s-indacene.** **5** was synthesized following the general procedure using 600 mg (3.79 mmol) of 3,5-difluoro-4-hydroxybenzaldehyde and purified using silica column chromatography using DCM as eluent. 419 mg, 25 % Yield.  $^1H$ -NMR (400 MHz DMSO- $d_6$ )  $\delta$  = 10.64 (s, 1H), 7.15 (dd, 2H,  $J$  = 7.1, 1.5 Hz), 2.43 (s, 6H), 2.31 (q, 4H,  $J$  = 7.6 Hz), 1.39 (s, 6H), 0.95 (t, 6H,  $J$  = 7.6 Hz).  $^{13}C$ -NMR (100 MHz DMSO- $d_6$ ) 153.6, 153.4, 152.0, 137.8, 134.3, 132.6, 130.0, 124.4, 112.4, 16.3, 14.4, 12.1, 11.4  $\delta$  ppm. HR-MS (ESI+):  $m/z$  calculated for  $C_{23}H_{26}BF_4N_2O$   $[M+H]^+$ : 433.2074, found: 433.2018.

**Dye 6. 8-(3-chloro-5-fluoro-4-hydroxyphenyl)-1,3,5,7-tetramethyl-2,6-diethyl-4,4-difluoro-4-bora-3a,4a-diaza-s-indacene.** **6** was synthesized following the general procedure using 100 mg (0.57 mmol) of 3-chloro-5-fluoro-4-hydroxybenzaldehyde and purified using silica column chromatography using  $CH_2Cl_2$  as eluent. 56 mg, 22 % yield.  $^1H$  NMR (600 MHz, Chloroform- $d$ )  $\delta$  7.11 (t,  $J$  = 1.8 Hz, 1H), 7.01 (dd,  $J$  = 10.0, 2.0 Hz, 1H), 5.82 (s, 1H), 2.53 (d,  $J$

= 1.1 Hz, 6H), 2.31 (q,  $J = 7.6$  Hz, 4H), 1.41 (s, 6H), 0.99 (t,  $J = 7.6$  Hz, 6H).  $^{13}\text{C}$  NMR (151 MHz,  $\text{CDCl}_3$ )  $\delta$  154.61, 152.47, 150.83, 141.11, 141.01, 137.89, 136.42, 133.23, 130.64, 128.20, 128.14, 124.98, 124.95, 122.47, 122.45, 115.54, 115.41, 17.07, 14.59, 12.57, 12.10. HR-MS (ESI+):  $m/z$  calculated for  $\text{C}_{23}\text{H}_{26}\text{BClF}_3\text{N}_2\text{O}$   $[\text{M}+\text{H}]^+$ : 449.1779, found: 449.1742.

**Dye 7. 8-(4-hydroxy-3-(trifluoromethyl)phenyl)-1,3,5,7-tetramethyl-2,6-diethyl-4,4-difluoro-4-bora-3a,4a-diaza-s-indacene.** **7** was synthesized following the general procedure using 200 mg (1.05 mmol) of 4-hydroxy-3-(trifluoromethyl)benzaldehyde and purified using silica column chromatography using DCM:PE (90:10) as eluent. 138 mg, 28 % Yield.  $^1\text{H}$ -NMR (600 MHz  $\text{DMSO-d}_6$ )  $\delta$  = 11.04 (s, 1H), 7.47 (d, 1H,  $J = 2.1$  Hz), 7.32 (dd, 1H,  $J = 8.4, 2.2$  Hz), 7.20 (d, 1H,  $J = 8.4$  Hz), 2.43 (s, 6H), 2.29 (q, 4H,  $J = 7.6$  Hz), 1.31 (s, 6H), 0.94 (t, 6H,  $J = 7.6$  Hz).  $^{13}\text{C}$ -NMR (150 MHz  $\text{DMSO-d}_6$ )  $\delta$  156.4, 153.3, 139.0, 137.8, 133.7, 132.6, 130.3, 126.4, 124.6, 122.7, 117.8, 116.3, 16.3, 14.4, 12.1, 11.5 ppm. HR-MS (ESI+):  $m/z$  calculated for  $\text{C}_{24}\text{H}_{27}\text{BF}_5\text{N}_2\text{O}$   $[\text{M}+\text{H}]^+$ : 465.2137, found: 465.2256.

**Dye 8. 8-(2-chloro-4-hydroxyphenyl)-1,3,5,7-tetramethyl-2,6-diethyl-4,4-difluoro-4-bora-3a,4a-diaza-s-indacene.** **8** was synthesized following the general procedure using 234 mg (1.5 mmol) of 2-chloro-4-hydroxybenzaldehyde and product was purified by column chromatography on silica using PE/ $\text{CH}_2\text{Cl}_2$  4:1 as eluent to give the compound as purple solid (129 mg, 20%).  $^1\text{H}$  NMR (600 MHz, Chloroform- $d$ )  $\delta$  7.11 (d,  $J = 8.3$  Hz, 1H), 7.01 (d,  $J = 2.4$  Hz, 1H), 6.87 (dd,  $J = 8.3, 2.5$  Hz, 1H), 2.53 (d,  $J = 1.1$  Hz, 6H), 2.31 (q,  $J = 7.6$  Hz, 4H), 1.40 (s, 6H), 1.00 (t,  $J = 7.6$  Hz, 6H).  $^{13}\text{C}$  NMR (151 MHz,  $\text{CDCl}_3$ )  $\delta$  156.94, 154.09, 137.91, 136.33, 133.86, 132.75, 130.94, 130.82, 126.88, 116.96, 115.11, 17.09, 14.65, 12.58, 11.02. HR-MS (ESI+):  $m/z$  calculated for  $\text{C}_{23}\text{H}_{27}\text{BClF}_2\text{N}_2\text{O}$   $[\text{M}+\text{H}]^+$ : 431.1873, found 431.1873.

**Dye 9. 8-(4-hydroxyphenyl)-1,3,5,7-tetramethyl-2,6-diethyl-4,4-difluoro-4-bora-3a,4a-diaza-s-indacene.** This dye was synthesized according to ref. 30 with a yield of 45%. <sup>1</sup>H-NMR (300 MHz, CDCl<sub>3</sub>) δ 0.98 (t, 6H, *J* = 7.6 Hz), 1.35 (s, 6H), 2.30 (q, 4H, *J* = 7.6 Hz), 2.53 (s, 6H), 6.94 (m, 2H), 7.12 (m, 2H). <sup>13</sup>C-NMR (75 MHz, CDCl<sub>3</sub>) δ 12.0, 12.6, 14.8, 17.2, 116.1, 128.1, 129.9, 131.3, 132.0, 138.6, 140.3, 153.7, 156.3 ppm. HR-MS (ESI+): *m/z* calculated for C<sub>23</sub>H<sub>27</sub>BF<sub>2</sub>N<sub>2</sub>O: 396.2185, found: 396.2248.

**Dye 10. 8-(3,5-di-*tert*-butyl-4-hydroxyphenyl)-1,3,5,7-tetramethyl-2,6-diethyl-4,4-difluoro-4-bora-3a,4adiaza-s-indacene. 10** was synthesized following the general procedure using 1.582 mg (6.5 mmol) of 3,5-ditertbutyl-4-hydroxybenzaldehyde and purified using silica column chromatography using EtOAc:PE (1:99) as eluent. 354 mg, 11 % Yield. <sup>1</sup>H-NMR (500 MHz CDCl<sub>3</sub>) δ = 7.12 (s, 2H), 2.56 (s, 6H), 2.34 (q, 4H, *J* = 7.6 Hz), 1.47 (s, 18H), 1.34 (s, 6H), 1.03 (t, 6H, *J* = 7.6 Hz). <sup>13</sup>C-NMR (125 MHz CDCl<sub>3</sub>) δ 154.3, 153.3, 142.0, 138.5, 137.2, 132.6, 131.4, 126.5, 124.8, 34.7, 17.3, 14.8, 12.6, 11.7 ppm. HR-MS (ESI+): *m/z* calculated for C<sub>31</sub>H<sub>44</sub>BOF<sub>2</sub>N<sub>2</sub> [M+H]<sup>+</sup>: 509.3509, found: 509.3520.

**Dye In1. 8-(2,6-dimethylpyridin-4-yl)-1,3,5,7-tetramethyl-2,6-diethyl-4,4-difluoro-4-bora-3a,4adiaza-s-indacene. In1** was synthesized following the general procedure with 500 mg (3.94 mmol) of 2,6-dimethyl-4-pyridinecarboxyaldehyde and purified using silica column chromatography CH<sub>2</sub>Cl<sub>2</sub>:EtOAc (96:4) as eluent. 342 mg, 21 % Yield. <sup>1</sup>H-NMR (400 MHz DMSO-d<sub>6</sub>) δ =7.12 (s, 2H), 2.49 (s, 6H), 2.42 (s, 6H), 2.28 (q, 4H, *J* = 7.4 Hz), 1.32 (s, 6H), 0.93 (t, 6H, *J* = 7.4 Hz) ppm. <sup>13</sup>C-NMR (100 MHz DMSO-d<sub>6</sub>) δ 158.4, 153.7, 150.6, 143.4, 137.8, 132.9, 119.5, 119.5, 23.9, 16.4, 14.5, 12.3, 11.6 ppm. HR-MS (ESI+): *m/z* calculated for C<sub>24</sub>H<sub>31</sub>BF<sub>2</sub>N<sub>3</sub> [M+H]<sup>+</sup>: 410.2579, found: 410.2329.

**Dye In2. 8-(4-bis(2-methoxyethyl)aminophenyl)-1,3,5,7-tetramethyl-2,6-diethyl-4,4-difluoro-4-bora-3a,4a-diaza-s-indacene.** In2 was synthesized following the general procedure with 65mg (0.27mmol) of A2 and purified using silica column chromatography with DCM as eluent. 28mg, 20 % yield. <sup>1</sup>H NMR (600 MHz, Chloroform-*d*) δ 7.09 (d, *J* = 8.1 Hz, 2H), 6.95 (bs, 2H), 3.67 – 3.60 (m, 8H), 3.36 (s, 6H), 2.52 (s, 6H), 2.31 (q, *J* = 7.6 Hz, 4H), 1.38 (s, 6H), 0.99 (t, *J* = 7.5 Hz, 6H). <sup>13</sup>C NMR (151 MHz, CDCl<sub>3</sub>) δ 153.19, 149.50, 140.90, 138.41, 132.49, 131.35, 129.33, 122.79, 114.56, 69.56, 66.81, 59.04, 17.10, 14.65, 12.46, 11.98. HR-MS (ESI+): *m/z* calculated for C<sub>29</sub>H<sub>41</sub>BF<sub>2</sub>N<sub>3</sub>O<sub>2</sub> [M+H]<sup>+</sup>: 512.3260, found: 512.3084.

**Dye In3. 8-(4-aminophenyl)-1,3,5,7-tetramethyl-2,6-diethyl-4,4-difluoro-4-bora-3a,4a-diaza-s-indacene.** This dye was synthesized according to ref. 38 using CH<sub>2</sub>Cl<sub>2</sub>/MeOH as solvent and 0.1 equivalents of 10% Pd/C. With this slight modification, a 99% yield was obtained. <sup>1</sup>H NMR (600 MHz, Chloroform-*d*) δ 7.03 (d, *J* = 7.8 Hz, 2H), 6.86 (d, *J* = 7.7 Hz, 2H), 2.52 (s, 6H), 2.29 (q, *J* = 7.6 Hz, 4H), 1.38 (s, 6H), 0.97 (t, *J* = 7.6 Hz, 6H). <sup>13</sup>C NMR (151 MHz, CDCl<sub>3</sub>) δ 153.28, 145.66, 140.80, 138.46, 132.52, 131.29, 129.27, 126.42, 116.11, 17.08, 14.64, 12.46, 11.93. HR-MS (ESI+): *m/z* calculated for C<sub>23</sub>H<sub>29</sub>BF<sub>2</sub>N<sub>3</sub> [M+H]<sup>+</sup>: 396.2423, found: 396.2389.

**Dye In4. 8-(4-diethylaminophenyl)-1,3,5,7-tetramethyl-2,6-diethyl-4,4-difluoro-4-bora-3a,4a-diaza-s-indacene.** In4 was synthesized following the general procedure using 200 mg (1.05 mmol) of 4-diethylaminobenzaldehyde and purified by column chromatography on silica using PE/CH<sub>2</sub>Cl<sub>2</sub> 7:3 as eluent to give the desired compound as red solid (250 mg, 18%). <sup>1</sup>H NMR (600 MHz, Chloroform-*d*) δ 7.02 (d, *J* = 8.1 Hz, 2H), 6.75 (s, 2H), 3.41 (q, *J* = 7.1 Hz, 4H), 2.52 (s, 6H), 2.31 (q, *J* = 7.6 Hz, 4H), 1.42 (s, 6H), 1.20 (t, *J* = 7.1 Hz, 6H), 0.99 (t, *J* = 7.6 Hz, 6H). <sup>13</sup>C NMR (151 MHz, CDCl<sub>3</sub>) δ 152.82, 148.03, 141.82, 138.61, 132.30, 131.57, 129.18, 122.12,

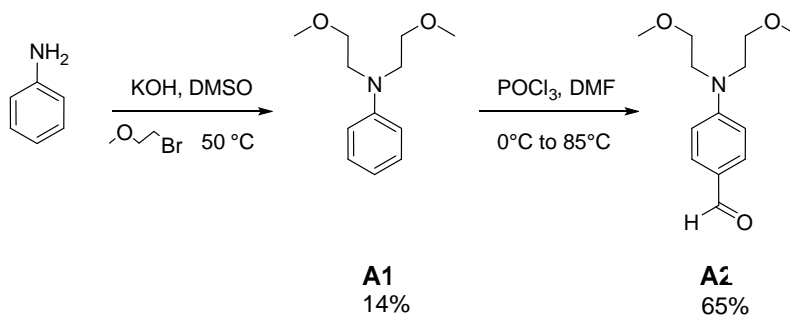
112.05, 44.39, 29.70, 17.11, 14.67, 12.44, 11.97. HR-MS (ESI+):  $m/z$  calculated for  $C_{27}H_{37}BF_2N_3$   $[M+H]^+$ : 452.3049, found 452.3009.

**Dye In5. 8-(4'-(diethylamino)-[1,1'-biphenyl]-4-yl)-1,3,5,7-tetramethyl-2,6-diethyl-4,4-difluoro-4-bora-3a,4a-diaza-s-indacene.** *meso*-Bromophenyl-bodipy **A4** (91.8 mg, 0.20 mmol), 4-(diethylamino)phenylboronic acid (115.8 mg, 0.6 mmol) and potassium carbonate (165.8 mg, 1.2 mmol) were dissolved in 10 mL of a DMF–water (4/1 v/v) mixture. Argon was sparkled for 10 min and then (triphenylphosphine)palladium(0) (11.5 mg, 10  $\mu$ mol) was added. The mixture was degassed for 5 more minutes and heated to 100 °C. After 1 hr., TLC revealed quantitative consumption of starting materials. Solvents were then evaporated and the mixture was dissolved in dichloromethane. The organic solvent was washed twice with water, and the aqueous layer was extracted with dichloromethane. The combined organic layers were washed with NaCl (sat.) and dried with  $Na_2SO_4$ . After solvent evaporation, the remaining mixture was purified by silica column chromatography using EtOAc–hexane 2 : 8 as eluent. 84 mg, yield 80%.  $^1H$ -NMR (500 MHz  $CDCl_3$ )  $\delta$  = 7.69 (d, 2H,  $J$  = 8.2 Hz), 7.59 (d, 2H,  $J$  = 8.9 Hz), 7.26 (d, 2H,  $J$  = 8.2 Hz), 6.79 (d, 2H,  $J$  = 8.9 Hz), 3.43 (q, 4H,  $J$  = 7.1 Hz), 2.56 (s, 6H), 2.31 (q, 4H,  $J$  = 7.5 Hz), 1.37 (s, 6H), 1.21 (t, 6H,  $J$  = 7.1 Hz), 0.98 (t, 6H,  $J$  = 7.5 Hz).  $^{13}C$ -NMR (125 MHz  $CDCl_3$ )  $\delta$  153.6, 147.6, 141.5, 140.7, 138.7, 133.1, 132.8, 131.1, 128.7, 127.8, 126.7, 126.3, 112.2, 44.6, 17.2, 14.8, 12.7, 12.6, 12.0 ppm. HR-MS (ESI+):  $m/z$  calculated for  $C_{33}H_{41}BF_2N_3$   $[M+H]^+$ : 528.3362, found: 528.3367.

**Dye In6. 8-(4-di-(*iso*-propyl)aminophenyl)-1,3,5,7-tetramethyl-2,6-diethyl-4,4-difluoro-4-bora-3a,4a-diaza-s-indacene.** **In6** was synthesized following the general procedure with 160 mg (0.82 mmol) of **A3** and purified using silica column chromatography using DCM as eluent. 88 mg, 21%. Yield  $^1H$  NMR (600 MHz,  $DMSO-d_6$ )  $\delta$  7.05 (d,  $J$  = 8.7 Hz, 2H), 6.98 (d,  $J$  = 8.7 Hz, 2H), 3.83 (h,  $J$  = 6.8 Hz, 2H), 2.42 (s, 6H), 2.29 (q,  $J$  = 7.7 Hz, 4H), 1.39 (s, 6H), 1.21 (d,  $J$  = 6.7

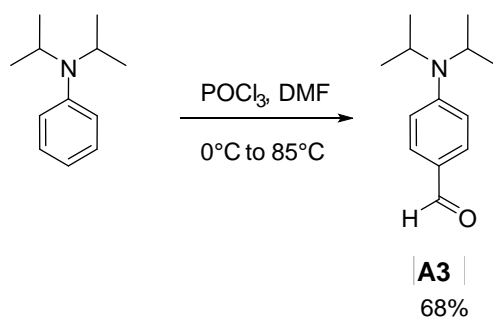
Hz, 12H), 0.94 (t,  $J = 7.5$  Hz, 6H).  $^{13}\text{C}$  NMR (151 MHz, DMSO)  $\delta$  152.90, 148.77, 142.17, 138.61, 132.74, 131.02, 128.58, 123.64, 118.77, 47.40, 21.36, 15.02, 14.36, 11.98, 11.28. HR-MS (ESI+):  $m/z$  calculated for  $\text{C}_{29}\text{H}_{41}\text{BF}_2\text{N}_3$   $[\text{M}+\text{H}]^+$ : 480.3362, found: 480.2108.

**Dye In7. 8-(4-hydroxy-3-methoxy-5-nitrophenyl)-1,3,5,7-tetramethyl-2,6-diethyl-4,4-difluoro-4-bora-3a,4a-diaza-s-indacene. In7** was synthesized following the general procedure and purified using silica column chromatography using DCM:PE (60:40) as eluent. 269 mg, 25 % Yield.  $^1\text{H}$ -NMR (400 MHz DMSO- $d_6$ )  $\delta$  = 10.78 (s, 1H), 7.43 (d, 1H,  $J = 2.0$  Hz), 7.31 (d, 1H,  $J = 2.0$  Hz), 3.89 (s, 3H), 2.44 (s, 6H), 2.31 (q, 4H,  $J = 7.5$  Hz), 1.42 (s, 6H), 0.95 (t, 6H,  $J = 7.6$  Hz).  $^{13}\text{C}$ -NMR (100 MHz DMSO- $d_6$ )  $\delta$  153.5, 150.3, 142.3, 138.0, 138.0, 137.9, 132.6, 130.0, 124.5, 115.8, 115.6, 57.0, 16.3, 14.7, 12.1, 11.6. ppm. HR-MS (ESI+):  $m/z$  calculated for  $\text{C}_{24}\text{H}_{29}\text{BF}_2\text{N}_3\text{O}_4$   $[\text{M}+\text{H}]^+$ : 472.2219, found: 472.0508.



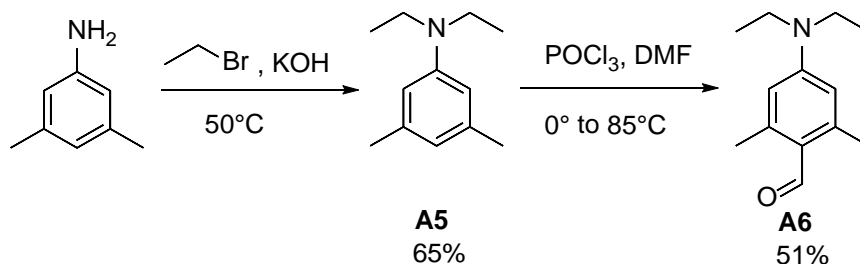
**Compound A1. *N,N*-bis(2-methoxyethyl)aniline.** Freshly distilled aniline (0.500 mL, 5.48 mmol), 2-bromoethyl methyl ether (2.06 mL, 21.94 mmol) and KOH (616 mg, 10.97 mmol) in 20 ml DMSO were stirred for 18 hr at 50 °C. Then, mixture was poured into water, neutralized with HCl 1M and extracted 3 times with EtOAc. The organic layer was then washed with NaCl(sat) and dried with Na<sub>2</sub>SO<sub>4</sub>. Solvents were then evaporated and the mixture was purified by column chromatography using 9:1 to 88:12 PE:EtOAc as eluent obtaining 159 mg (14% yield) of a brownish oil. HR-MS (ESI<sup>+</sup>): *m/z* calculated for C<sub>12</sub>H<sub>20</sub>NO<sub>2</sub> [M+H]<sup>+</sup>: 210.1494, found: 210.0784.

**Compound A2. 4-(bis(2-methoxyethyl)amino)benzaldehyde.** A mixture of anhydrous 5 ml DMF and POCl<sub>3</sub> (78 uL, 0.84 mmol) was stirred under a nitrogen atmosphere at 0 °C for 1.5 hr. and then at room temperature for additional 1 hr. The yellow solution was then heated at 85 °C. Aniline **A1** (0.76 mmol, 159 mg) was added and the resulting mixture was stirred at 85 °C for 4 more hr. The solvent was then removed under reduced pressure, and the residue was dissolved in 50 ml of water and the pH was adjusted to 7-8 by the addition of NaHCO<sub>3</sub>(sat) solution. The aqueous phase was extracted with DCM (3 × 50 ml) and then the combined organic phases were washed with water (2 x 50 ml), dried over Na<sub>2</sub>SO<sub>4</sub> and the solvent evaporated under reduced pressure. The residue was purified by column chromatography (Silica, PE:EtOAc 7:3 to 66:24) to afford 119 mg (65 % yield) of the title compound. HR-MS (ESI<sup>+</sup>): *m/z* calculated for C<sub>13</sub>H<sub>20</sub>NO<sub>3</sub> [M+H]<sup>+</sup>: 238.1443, found: 238.0540.



**Compound A3. 4-(diisopropylamino)benzaldehyde.** A mixture of anhydrous 5 ml DMF and POCl<sub>3</sub> (132 μL, 1.41 mmol) was stirred under a nitrogen atmosphere at 0 °C for 1.5 hr. and then at room temperature for additional 1 hr. The yellow solution was then heated at 85 °C. Diisopropylaniline (1.28 mmol, 0.25 mL) was added and the resulting mixture was stirred at 85 °C for 4 more hr. The solvent was then removed under reduced pressure, and the residue was dissolved in 50 ml of water and the pH was adjusted to 7-8 by the addition of NaHCO<sub>3</sub>(sat) solution. The aqueous phase was extracted with DCM (3 × 50 mL) and then the combined organic phases were washed with water (2 × 50 mL), dried over Na<sub>2</sub>SO<sub>4</sub> and the solvent evaporated under reduced pressure. The residue was purified by column chromatography (Silica, PE:EtOAc 86:14) to afford 179 mg (67 % yield) of the title compound. HR-MS (ESI<sup>+</sup>): *m/z* calculated for C<sub>13</sub>H<sub>20</sub>NO [M+H]<sup>+</sup>: 206.1545, found: 206.0554.

**Compound A4. 8-(4-Bromophenyl)-4,4-difluoro-1,3,5,7-tetramethyl-2,6-diethyl-4-bora-3a,4a-diaza-s-indacene. A4** was synthesized according to ref. 39. 43 % yield. HR-MS (ESI<sup>+</sup>): *m/z* calculated for C<sub>26</sub>H<sub>26</sub>BBrF<sub>2</sub>N<sub>2</sub> [M+H]<sup>+</sup>: 457.1368, found: 457.1371.



**Compound A5. *N,N'*-(Diethylamino)-3,5-dimethylaniline.** 3,5-Dimethylaniline (484 mg, 4 mmol) was dissolved in 16 mL DMSO. Then, ethylbromide (1.74 g, 16 mmol) was added, followed by KOH (448 mg, 8 mmol). The mixture was heated to 50 °C and allowed to react overnight. After evaporation of the solvent, the mixture was re-dissolved in Et<sub>2</sub>O and washed two times with NaHCO<sub>3</sub> 10% and then with NaCl(sat.). After drying with MgSO<sub>4</sub>, the solvent was evaporated and the mixture purified by column chromatography using PE:EtOAc 9:1 as eluent. Yield: 65 %. <sup>1</sup>H-NMR (400 MHz CDCl<sub>3</sub>) δ = 6.33 (s, 3H), 3.33 (q, 4H, J = 7.0 Hz), 2.27 (s, 6H), 1.15 (t, 6H, J = 7.0 Hz).

**Compound A6. 4-(Diethylamino)-2,6-dimethylbenzaldehyde.** **A6** was synthesized following a similar procedure detailed for compound **A3** above. Yield: 51 %. <sup>1</sup>H-NMR (500 MHz CDCl<sub>3</sub>) δ = 10.32 (s, 1H), 6.28 (s, 2H), 3.40 (q, 4H, J = 6.9 Hz), 2.59 (s, 6H), 1.20 (t, 6H, J = 7.3 Hz). <sup>13</sup>C-NMR (125 MHz CDCl<sub>3</sub>) δ 190.1, 150.7, 144.5, 121.0, 111.4, 44.3, 21.7, 12.7 ppm.

## S10. References

- 1 Aigner, D.; Borisov, S. M.; Klimant, I. *Anal. Bioanal. Chem.* **2011**, *400*, 2475-2485.
- 2 Tsou, C.-J.; Chu, C.; Hung, Y.; Mou, C.-Y. *J. Mater. Chem. B* **2013**, *1*, 5557-5563.
- 3 Lin, J.; Liu, D. *Anal. Chim. Acta* **2000**, *408*, 49-55.
- 4 Kumar, P. E. K.; Fedborg, L. N.; Almdal, K.; Andresen, T. L. *Chem. Mater.* **2013**, *25*, 1496-1501.
- 5 McDonnell, S. O.; O'Shea, D. F. *Org. Lett.* **2006**, *8*, 3493-3496.
- 6 Sansalvador, I. M. P. d. V.; Fay, C. D.; Cleary, J.; Nightingale, A. M.; Mowlem, M. C.; Diamond, D. *Sens. Actuators B* **2016**, *225*, 369-376.
- 7 Zhang, X.; Li, Z.; Zhou, T.; Zhou, Q.; Zeng, Z.; Xu, X.; Hu, Y. *Talanta* **2016**, *150*, 184-189.
- 8 Zhang, M.; Sondergaard, R. V.; Kumar, E. K. P.; Henriksen, J. R.; Cui, D.; Hammershoj, P.; Clausen, M. H.; Andresen, T. L. *Analyst* **2015**, *140*, 7246-7253.
- 9 Tsou, C.-J.; Hung, Y.; Mou, C.-Y. *Microporous Mesoporous Mater.* **2014**, *190*, 181-188.
- 10 Meier, R. J.; Simbuerger, J. M. B.; Soukka, T.; Schaeferling, M. *Chem. Commun.* **2015**, *51*, 6145-6148.
- 11 Chu, B.; Wang, H.; Song, B.; Peng, F.; Su, Y.; He, Y. *Anal. Chem.* **2016**, *88*, 9235-9242.
- 12 Netto, E. J.; Peterson, J. I.; McShane, M.; Hampshire, V. *Sens. Actuators B* **1995**, *29*, 157-163.
- 13 Strobl, M.; Rappitsch, T.; Borisov, S. M.; Mayr, T.; Klimant, I. *Analyst* **2015**, *140*, 7150-7153.
- 14 Niu, C. G.; Gui, X. Q.; Zeng, G. M.; Yuan, X. Z. *Analyst* **2005**, *130*, 1551-1556.
- 15 Aguilera-Sigalat, J.; Bradshaw, D. *Chem. Commun.* **2014**, *50*, 4711-4713.
- 16 Qian, Z.; Ma, J.; Shan, X.; Feng, H.; Shao, L.; Chen, J. *Chem. Eur. J.* **2014**, *20*, 2254-2263.
- 17 Cui, H.; Chen, Y.; Li, L.; Wu, Y.; Tang, Z.; Fu, H.; Tian, Z. *Microchim. Acta* **2014**, *181*, 1529-1539.
- 18 Dong, S.; Luo, M.; Peng, G.; Cheng, W. *Sens. Actuators B* **2008**, *129*, 94-98.
- 19 Khodadoust, S.; Kouri, N. C.; Talebiyanpoor, M. S.; Deris, J.; Pebdani, A. A. *Mater. Sci. Eng. C* **2015**, *57*, 304-308.
- 20 Chen, S.; Liu, J.; Liu, Y.; Su, H.; Hong, Y.; Jim, C. K. W.; Kwok, R. T. K.; Zhao, N.; Qin, W.; Lam, J. W. Y.; Wong, K. S.; Tang, B. Z. *Chem. Sci.* **2012**, *3*, 1804-1809.
- 21 Shamsipur, M.; Abbasitabar, F.; Zare-Shahabadi, V.; Akhond, M. *Anal. Lett.* **2008**, *41*, 3113-3123.
- 22 Vasylevska, A. S.; Karasyov, A. A.; Borisov, S. M.; Krause, C. *Anal. Bioanal. Chem.* **2007**, *387*, 2131-2141.
- 23 Qi, J.; Liu, D.; Liu, X.; Guan, S.; Shi, F.; Chang, H.; He, H.; Yang, G. *Anal. Chem.* **2015**, *87*, 5897-5904.

- 24 Capel-Cuevas, S.; Cuellar, M. P.; de Orbe-Paya, I.; Pegalajar, M. C.; Capitan-Vallvey, L. F. *Anal. Chim. Acta* **2010**, *681*, 71-81.
- 25 Shen, Z.; Röhr, H.; Rurack, K.; Uno, H.; Spieles, M.; Schulz, B.; Reck, G.; Ono, N. *Chem. Eur. J.* **2004**, *10*, 4853-4871.
- 26 Resch, U.; Rurack, K. *Proc. SPIE-Int. Soc. Opt. Eng.* **1997**, *3105*, 96-103.
- 27 Kaltofen, R.; Optiz, R.; Schumann, K.; Ziemann, J. Tabellenbuch Chemie, VEB Deutscher Verlag für Grundstoffindustrie, Leipzig, 2nd Edn, 1982.
- 28 Gaussian 03, Revision D.01, Frisch, M. J.; Trucks, G. W.; Schlegel, H. B.; Scuseria, G. E.; Robb, M. A.; Cheeseman, J. R.; Montgomery, Jr., J. A.; Vreven, T.; Kudin, K. N.; Burant, J. C.; Millam, J. M.; Iyengar, S. S.; Tomasi, J.; Barone, V.; Mennucci, B.; Cossi, M.; Scalmani, G.; Rega, N.; Petersson, G. A.; Nakatsuji, H.; Hada, M.; Ehara, M.; Toyota, K.; Fukuda, R.; Hasegawa, J.; Ishida, M.; Nakajima, T.; Honda, Y.; Kitao, O.; Nakai, H.; Klene, M.; Li, X.; Knox, J. E.; Hratchian, H. P.; Cross, J. B.; Bakken, V.; Adamo, C.; Jaramillo, J.; Gomperts, R.; Stratmann, R. E.; Yazyev, O.; Austin, A. J.; Cammi, R.; Pomelli, C.; Ochterski, J. W.; Ayala, P. Y.; Morokuma, K.; Voth, G. A.; Salvador, P.; Dannenberg, J. J.; Zakrzewski, V. G.; Dapprich, S.; Daniels, A. D.; Strain, M. C.; Farkas, O.; Malick, D. K.; Rabuck, A. D.; Raghavachari, K.; Foresman, J. B.; Ortiz, J. V.; Cui, Q.; Baboul, A. G.; Clifford, S.; Cioslowski, J.; Stefanov, B. B.; Liu, G.; Liashenko, A.; Piskorz, P.; Komaromi, I.; Martin, R. L.; Fox, D. J.; Keith, T.; Al-Laham, M. A.; Peng, C. Y.; Nanayakkara, A.; Challacombe, M.; Gill, P. M. W.; Johnson, B.; Chen, W.; Wong, M. W.; Gonzalez, C.; Pople, J. A., Gaussian, Inc., Wallingford CT, 2004.
- 29 Gross, K. C.; Seybold, P. G.; Hadad, C. M. *Int. J. Quantum Chem.* **2002**, *90*, 445-458.
- 30 Hecht, M.; Kraus, W.; Rurack, K. *Analyst* **2013**, *138*, 325-332.
- 31 Wang, Y.-W.; Descalzo, A. B.; Shen, Z.; You, X.-Z.; Rurack, K. *Chem. Eur. J.* **2010**, *16*, 2887-2903.
- 32 Fairman, H.S.; Brill, M. H.; Hemmendinger, H. *Color Res. Appl.* **1997**, *22*, 11-23.
- 33 Smith, A. R. *SIGGRAPH 78 Conf. Proc.* **1978**, 12-19. Tutorial: *Computer Graphics*, Beatty, J. C., Booth, K. S., Eds.; IEEE Computer Society Press, 2nd Edn, 1982; pp 376-383.
- 34 XDA-Developers. The promise of RAW smartphone photography. <https://www.xda-developers.com/the-promise-of-raw-smartphone-photography> (accessed May 10, 2017).
- 35 Android Developers. Reference: Image Format. <https://developer.android.com/reference/android/graphics/ImageFormat.html#RAW10> (accessed May 10, 2017).
- 36 M. J. Frisch, et al., Gaussian 09 (Gaussian, Inc., Wallingford CT, 2009).
- 37 Coskun, A.; Akkaya, E. U. *J. Am. Chem. Soc.* **2005**, *127*, 10464-10465.
- 38 Ziessel, R.; Bonardi, L.; Retailleau, P.; Ulrich, G. *J. Org. Chem.* **2006**, *71*, 3093-3102.
- 39 Benniston, A. C.; Copley, G.; Elliott, K. J.; Harrington, R. W.; Clegg, W. *Eur. J. Org. Chem.* **2008**, 2705- 2713.